

Correlation between South China and India and development of double rift systems in the South China-India Duo during late Neoproterozoic time

Touping Peng¹, Bingbing Liu¹, Weiming Fan², Guochun Zhao³, Jianfeng Gao⁴, Xiaohan Dong¹, Shili Peng¹, Limin Wu¹, and Bingxia Peng¹

¹a. State Key Laboratory of Isotope Geochemistry, Guangzhou Institute of Geochemistry, Chinese Academy of Sciences

²University of Chinese Academy of Sciences

³The University of Hong Kong

⁴Institute of Geochemistry, Chinese Academy of Sciences

November 23, 2022

Abstract

South China, India and their derivative terranes/blocks preserve a larger amount of similar magmatic and sedimentary records related to the tectonic transition from Rodinia to Gondwana. They provide crucial insights into not only the paleogeographic correlation between them but also the geodynamic mechanism for such a transition. Our new results together with published big data from these terranes/blocks point out that South China kept a linkage with India at least from the late Tonian (ca. 830 Ma) to Early Cambrian and formed the South China-India Duo located at the western margin of Rodinia. The identical magmatism and sedimentation reflect that double late Neoproterozoic rift systems in the South China-India Duo could have developed owing to the rollback of subducting oceanic slab beneath them, including an intracontinental rift (the Nanhua-Aravalli-Delhi rift) separating the Yangtze-Marwar from Cathaysia-Bundelkhand terranes and a contemporaneous intra-arc rift along the northern and western margins of the Yangtze Terrane, through the Marwar Terrane of western India, and then into the Seychelles and Madagascar terranes. Such an intra-arc rift is also the most feasible explanation for the common development of coeval arc-like and extension-related magmatic rocks and extensional sedimentary sequences on the western margin of the South China-India Duo and in Seychelles and Madagascar, and even other subduction zones.

24 **Abstract**

25 South China, India and their derivative terranes/blocks preserve a larger amount
26 of similar magmatic and sedimentary records related to the tectonic transition from
27 Rodinia to Gondwana. They provide crucial insights into not only the
28 paleogeographic correlation between them but also the geodynamic mechanism for
29 such a transition. Our new results together with published big data from these
30 terranes/blocks point out that South China kept a linkage with India at least from the
31 late Tonian (ca. 830 Ma) to Early Cambrian and formed the South China-India Duo
32 located at the western margin of Rodinia. The identical magmatism and sedimentation
33 reflect that double late Neoproterozoic rift systems in the South China-India Duo
34 could have developed owing to the rollback of subducting oceanic slab beneath them,
35 including an intracontinental rift (the Nanhua-Aravalli-Delhi rift) separating the
36 Yangtze-Marwar from Cathaysia-Bundelkhand terranes and a contemporaneous
37 intra-arc rift along the northern and western margins of the Yangtze Terrane, through
38 the Marwar Terrane of western India, and then into the Seychelles and Madagascar
39 terranes. Such an intra-arc rift is also the most feasible explanation for the common
40 development of coeval arc-like and extension-related magmatic rocks and extensional
41 sedimentary sequences on the western margin of the South China-India Duo and in
42 Seychelles and Madagascar, and even other subduction zones.

43 **Key words:** Detrital zircon U-Pb-Hf isotope, Neoproterozoic-Early Paleozoic
44 sedimentary sequences, South China-India Duo, late Neoproterozoic rift systems,
45 Proto-Tethys Ocean

46 **1. Introduction**

47 Supercontinent forms when nearly all continental blocks on earth collide with
48 each other and assemble into a solely large landmass (Zhao et al., 2018a). Rodinia and
49 Gondwana are the most important ones of supercontinents in Earth's history (Zhao et
50 al., 2018a). Increasing lines of evidence including reliable geological, paleomagnetic
51 and paleontological data have established that they formed ca. 1.00 Ga and ca. 0.55
52 Ga ago, respectively (e.g., Cawood et al., 2013, 2018, and references therein).
53 Although the paleogeographic position of major continental blocks in Rodinia and
54 Gondwana have been widely accepted (Cawood et al., 2018; Zhao et al., 2018a), the
55 reconstructions of some microcontinents in Rodinia and Gondwana and their tectonic
56 evolution during the transition from Rodinia to Gondwana remain unknown. In
57 particular, South China and India, as two important continental blocks in Asia, have
58 been documented to be involved in the tectonic evolution of both Rodinia and
59 Gondwana based on magmatic, sedimentary and paleontological evidence (e.g.,
60 Cawood et al., 2013, 2018; Jiang et al., 2003; Metcalfe, 2013; Yang et al., 2004; Zhao
61 et al., 2018b). Their paleogeographic position and correlation in Rodinia and
62 Gondwana and their tectonic affinity are still the subject of debate (Cawood et al.,
63 2013, 2018; Chen et al., 2021; Jiang et al., 2003; Metcalfe, 2013; Wang et al., 2017a,
64 2021; Yang et al., 2004; Yao et al., 2014; Zhao et al., 2018b). Additionally, the
65 tectonic framework and geodynamic mechanism for the tectonic evolution of
66 supercontinents particularly during the transition from Rodinia to Gondwana remain
67 unresolved (Cawood et al., 2018; Li et al., 2002; Wang et al., 2017a; Zhao et al.,

68 [2018b](#)). Fortunately, in recent years, a large number of data about
69 Neoproterozoic-Early Paleozoic magmatic rocks and sedimentary sequences related to
70 the tectonic evolution of these two landmasses in South China and India and even
71 their derivative terranes/blocks have been published ([Chen et al., 2021](#); [Wang et al.,](#)
72 [2017a, 2021](#); [Yao et al., 2014](#); [Zhao et al., 2018b](#)). A combination and further analysis
73 of these big data are crucial to decode the aforementioned issues.

74 In this contribution, we present new U-Pb and Lu-Hf isotopic analyses of detrital
75 zircons of late Tonian to Ordovician sedimentary sequences from the Eastern Yidun
76 subterrane of South China, and combined with other published big data from South
77 China and other Gondwana- and Rodinia-derived continents, in order to re-evaluate
78 the correlation between South China and India and decode their tectonic evolution
79 during the transition from Rodinia to Gondwana. A new reconstruction model that
80 South China was connected with India and formed the South China-India Duo during
81 late Tonian-early Cambrian time is suggested. The breakup time of South China from
82 Indian Gondwana after the Early Cambrian due to the opening of the Proto-Tethys
83 Ocean is further constrained. Also, we propose the development of double late
84 Neoproterozoic rift systems in the South China-India Duo, including an intra-arc rift
85 along its western margin, and another intracontinental one (the Nanhua-Aravalli-Delhi
86 rift) separating the Yangtze-Marwar from Cathaysia-Bundelkhand terranes in the
87 interior of the South China-India Duo.

88

89 2. Geological background and samples

90 South China was formed by the amalgamation between the Yangtze Terrane to the
91 northwest and the Cathaysia Terrane to the southeast along the Neoproterozoic
92 Jiangnan fold belt (Cawood et al., 2018; Zhao et al., 2011). To its north is the North
93 China Craton and to the southwest is the Indochina Block. It is bounded by the Yidun
94 and Songpan-Ganzê terranes of the Tibetan Plateau to the northwest. The geological
95 characteristics of the Yangtze and Cathaysia terranes have been summarized in detail
96 by some authors (e.g., Cawood et al., 2013, 2018; Chen et al., 2021; Zhao et al.,
97 2018b).

98 The Yidun Terrane is a microcontinent located between the Qiangtang and
99 Songpan-Ganzê terranes, which is considered to be part of the Yangtze Terrane before
100 the Mesozoic (BGMRSF, 1980, 1984). It is surrounded by two Paleo-Tethys suture
101 zones, the Jinshajiang suture to the west and the Ganzê-Litang suture to the east (Fig.
102 1a, b; BGMRSF, 1984; Peng et al., 2014). To its southeast is the Yangtze Terrane,
103 which is separated by the Longmenshan-Jinhe Fault (BGMRSF, 1984; Peng et al.,
104 2014). Based on the tectono-stratigraphical distinction on the two flanks of the
105 north-south-trending Xiangcheng-Geza Fault, the Yidun Terrane can be divided into
106 the Western Yidun subterrane (also known as the Zhongza massif; Peng et al., 2014)
107 and the Eastern Yidun subterrane (Fig. 1a, b; Peng et al., 2014).

108 The western subterrane consists mainly of greenschist to lower amphibolite
109 facies Paleozoic meta-sedimentary rocks intercalated with minor meta-volcanics
110 (BGMRSF, 1984). The eastern subterrane is dominated by Triassic volcano-clastic

111 rocks with minor Neoproterozoic-Paleozoic sedimentary successions in the southeast
112 (BGMRS, 1984). The oldest strata are greenschist-amphibolite facies Neoproterozoic
113 Qiasi Group exposed in the southeast region of the Eastern Yidun subterrane,
114 comprising a suite of metamorphosed Neoproterozoic volcano-sedimentary
115 succession that consists of meta-volcanic, schist, leptynite and marble (Fig. 1;
116 BGMRS, 1984). It can be divided into four segments from bottom to top based on its
117 lithologic association characteristics (Fig. 1c, d; BGMRS, 1984). Unconformably
118 overlying the Qiasi Group is late Neoproterozoic (Ediacaran) sequences, comprised of
119 sandstone, carbonate and dolostone (BGMRS, 1984). These strata are in turn
120 unconformably overlain by Early Cambrian carbonate intercalated with some
121 siliciclastics (BGMRS, 1984). Ordovician succession, including sandstone, siltstone
122 and slate (Fig. 1 c, d; BGMRS, 1984), unconformably overlies Lower Cambrian
123 strata, and is in turn unconformably overlain by Early Silurian slate and silicalite.
124 Above these strata are the Upper Paleozoic sedimentary rocks comprised of Devonian
125 schist, marble and sandstone, Carboniferous-Upper Permian limestone, Upper
126 Permian basalt and slate (BGMRS, 1984). These Upper Paleozoic strata are
127 unconformably overlain by the Mesozoic and Paleogene sedimentary rocks in some
128 places (Fig. 1c; BGMRS, 1984). In addition, voluminous Middle-Late Triassic
129 (230-206 Ma), and minor amount of Permian, Cretaceous and Cenozoic igneous rocks
130 are exposed in the Eastern Yidun subterrane (e.g., BGMRS, 1984; Peng et al., 2014).

131 A total of five samples were collected for zircon U-Pb ages and Hf isotope
132 analyses (Table 1 and Figs. 1 & 2). Two schist samples (10YD-93 and 10YD-97) were

133 collected from the fourth and third segments of the Qiasi Group, respectively ([Table 1](#)
134 [and Figs. 1 & 2](#)). One sandstone sample (10YD-100) was collected from the
135 Ediacaran Dengying Formation and a slate sample (10YD-102) and a schist sample
136 (10YD-99) were collected from the Ordovician strata ([Table 1 and Figs. 1 & 2](#)).

137

138 **3. Analytical methods**

139 ***3.1 LA-ICP-MS zircon U-Pb dating***

140 ca. 5 kg of each sample was crushed and milled, and then zircons were separated
141 using heavy-liquid and magnetic methods at the Laboratory of the Geological Team
142 of Hebei Province, China. Cathodoluminescence (CL) images were taken at the
143 Guangzhou Institute of Geochemistry, Chinese Academy of Sciences (GIG-CAS) for
144 inspecting internal structures of individual zircons and for selecting positions for
145 U-Pb and Lu-Hf isotope analyses. Detrital zircons of varying size and shape were
146 selected randomly, leaving out grains with obvious cracks or inclusions.

147 In situ zircon U-Pb dating was carried out using an Agilent 7700x ICPMS
148 coupled to a 193 nm ArF Excimer Laser ablation system (GeoLas 2005, Lambda
149 Physik), housed at the Jupu analysis Lab, Nanjing of China. Analytical procedures
150 were the same as those described by [Liu et al. \(2010\)](#). The frequency of laser system
151 was 10 Hz. Gas flow rate of highly purified He as the carrier gas was 0.7 L/mn;
152 auxiliary gas Ar was 1.13 L/mn. The spot diameter was 40 μm in size. Total
153 acquisition time of one spot was 45 s. Zircon 91500 was used as external standard for

154 U-Pb dating, and was analyzed twice every 5 analyses. Time-dependent drifts of
155 U-Th-Pb isotopic ratios were corrected using a linear interpolation (with time) for
156 every five analyses according to the variations of 91500 (i.e., 2 zircon 91500 + 5
157 samples) (Liu et al., 2010). Preferred U-Th-Pb isotopic ratios used for 91500 are from
158 Liu et al. (2010). Uncertainty of preferred values for the external standard 91500 was
159 propagated to the ultimate results of the samples. Correction of common lead
160 followed the method described by Liu et al. (2010). Data were processed with the
161 ICPMSDataCal program (Liu et al., 2010). Uncertainties on individual analyses in
162 data tables were reported at a 1σ level. Results were analyzed and plotted using
163 Isoplot 3.0 (Ludwig, 2012). Zircon ages younger than 1000 Ma were based on
164 $^{206}\text{Pb}/^{238}\text{U}$ ratios, and ages older than 1000 Ma were based on $^{207}\text{Pb}/^{206}\text{Pb}$ ratios. In
165 this study, we excluded zircon age analyses with >10% discordance (Dickinson &
166 Gehrels, 2009).

167

168 ***3.2 In-situ zircon Hf isotope analysis***

169 After the LA-ICP-MS zircon U-Pb dating, zircon Lu-Hf isotope compositions
170 were analyzed by a 193 nm Ar-F excimer laser ablation system (RESolution
171 M-50-LR) attached to a multi-collector ICPMS (Neptune Plus), at GIG-CAS. The Hf
172 isotopes were obtained with a beam diameter of 45 μm , pulse rate of 6 Hz, energy
173 density of 80 J/cm^2 and Ablation time was 29 s. Quality control was made by
174 measuring zircon standard Penglai for the unknown samples during the analyses to

175 evaluate the reliability of the analytical data, yielded weighted mean an average
176 $^{176}\text{Hf}/^{177}\text{Hf}$ ratio of 0.282892 ± 0.000010 (1 standard deviation), which is consistent
177 within errors with the reported values of 0.282906 ± 0.000010 . In situ Hf isotope
178 measurements were subsequently done on the same spots or the same age domains for
179 age determinations of the concordant grains, as guided by CL images. The initial Hf
180 isotopic ratios and crustal model ages were calculated using the dating results of the
181 same spots.

182

183 **4. Results**

184 *4.1 Zircon U-Pb geochronology*

185 The LA-ICP-MS U-Pb dating results of zircons for the studied samples are listed
186 in [Table S1](#). Most analyses were plotted on or near the concordia curve ([Fig. 3](#)). The
187 detrital zircon U-Pb ages from the Eastern Yidun subterrane in this study show
188 different age distribution patterns with unimodal detrital zircon pattern for the
189 Neoproterozoic samples but multimodal pattern for the Ordovician ones ([Fig. 3](#)).

190 Zircon grains from all the Neoproterozoic samples in the Eastern Yidun
191 subterrane are primarily euhedral and partly subeuhedral. All of them show magmatic
192 oscillatory zoning in CL images ([Fig. S1](#)). 278 of 280 analyses produced 90-100%
193 concordant ages, which were considered to be available for the following discussion.
194 They gave an age spectrum ranging from 960 Ma to 574 Ma, and each sample
195 displays a similar unimodal pattern with a single major age population at 800-760 Ma

196 (Table S1 and Fig. 3). Only one older age of ca. 960 Ma is present in the sample
197 10YD-97 (Table S1 and Fig. 3).

198 Most of zircon crystals from the Ordovician samples in the Eastern Yidun
199 subterrane are subeuhedral to subround while some grains are rounded. All the
200 analyzed zircon grains show magmatic oscillatory zoning in CL images (Fig. S1). 163
201 out of 165 analyses are less than 10% discordance, which are available for the
202 following discussion. The two Ordovician samples yielded U-Pb age varying from
203 3093 to 447 Ma. They share similar multimodal distribution patterns, with major age
204 populations at 600-500 Ma and 860-700 Ma and a subordinate age group at
205 2500-2400 Ma (Fig. 3). One difference is that the schist sample (10YD-99) has an
206 alternative Grenvillian age population at 1100-900 Ma (Fig. 3).

207 *4.2 Zircon Hf isotopic compositions*

208 A total of 230 analyses for these three Neoproterozoic samples of the Eastern
209 Yidun subterrane exhibit a wide range of initial $^{176}\text{Hf}/^{177}\text{Hf}$ ratios from 0.282248 to
210 0.283031 (Table S2). Among them, 215 spots have positive $\epsilon_{\text{Hf}}(t)$ values between +0.1
211 and +24.0 with T_{DM}^{C} ages at 1.57-0.77 Ga (Table S2 and Fig.4), compatible with
212 those of the Neoproterozoic igneous rocks along the western and northern margins of
213 the Yangtze Terrane (Zhao et al., 2011). Only two Neoproterozoic zircons gave
214 slightly negative $\epsilon_{\text{Hf}}(t)$ values of -2.1 and -1.2, respectively (Table S2 and Fig.4).

215 In the case of the Ordovician samples in the Eastern Yidun subterrane, a total of
216 75 analyses exhibit a wide range of initial $^{176}\text{Hf}/^{177}\text{Hf}$ ratios from 0.280824 to

217 0.282793, corresponding to large variations of $\epsilon_{\text{Hf}}(t)$ values (-25.9 to +35.0),
218 indicating a mixing products of the juvenile ($\epsilon_{\text{Hf}}(t)>0$) and old ($\epsilon_{\text{Hf}}(t)<0$) crustal rocks
219 (Table S2 and Fig. 4). The main age group of 650-500 Ma have similar $\epsilon_{\text{Hf}}(t)$ values
220 (-25.0 to +6.1) with those of the magmatic rocks in the Kuunga Orogen (Zhu et al.,
221 2011, and references therein), while the age cluster at 830-700 Ma yield similar $\epsilon_{\text{Hf}}(t)$
222 values (-13.4 to +16.5) to those of the coeval igneous rocks in the Jiangnan Orogen in
223 South China (Fig. 4; Yao et al., 2019). The 1100-900 Ma detrital zircons from the
224 schist sample (10YD-99) show $\epsilon_{\text{Hf}}(t)$ values ranging from -8.5 to +13.2, compatible
225 with those in the Eastern Ghats Orogen and CITZ (Bhowmik et al., 2012; Zhu et al.,
226 2011; and references therein). Minor ca. 2400 Ma zircons have variable $\epsilon_{\text{Hf}}(t)$ values
227 between -11.4 and +35.0.

228

229 **5. Discussion**

230 *5.1. Sedimentary provenance*

231 By comparison, a unimodal age distribution pattern of the Neoproterozoic schists
232 in the Eastern Yidun subterrane similar to those in the western Yangtze Terrane reflect
233 a common provenance for the late Tonian-Ediacaran strata (Fig. 5). Owing to the
234 absence of the Neoproterozoic moderate-felsic magmatic rocks within the Yidun
235 Terrane (Tian et al., 2020), these Neoproterozoic detrital materials cannot be sourced
236 from the interior of this terrane. In contrast, voluminous 0.86-0.70 Ga igneous rocks
237 are exposed along the northern and western margins of the Yangtze Terrane, such as

238 the Neoproterozoic Panxi-Hannan arc (Zhao et al., 2018b; Zhou et al., 2006).
239 Moreover, the Hf isotopic compositions of detrital zircons from these Neoproterozoic
240 samples are in a good agreement with those of magmatic zircons of the
241 Neoproterozoic igneous rocks from the Panxi-Hannan arc (Fig. 4). In addition, these
242 detrital zircons of our Neoproterozoic samples are euhedral with magmatic zoning
243 (Fig. S1), indicating a short-distance transport from its provenance. Hence, we suggest
244 that the Neoproterozoic detritus in the Eastern Yidun subterrane could be mainly
245 sourced from the coeval igneous rocks in the Panxi-Hannan arc along the western and
246 northern margins of the Yangtze Terrane.

247 In the case of the Ordovician samples, they show a multimodal pattern
248 distinguishable from the unimodal one of the Neoproterozoic samples (Fig. 3). Except
249 for a similar major age of ca. 0.83-0.70 Ga to those Neoproterozoic samples, for
250 instance, they possess main age groups at ca. 0.65-0.50 Ga, ca. 1.00-0.90 Ga and a
251 subordinate age group at ca. 2.40 Ga (Fig. 3). Alternatively, the 0.83-0.70 Ga zircons
252 of the Ordovician samples have distinguishable $\epsilon_{\text{Hf}}(t)$ values (-16.1 to +15.7) from
253 those of the Neoproterozoic samples (Table S2), but are similar to those of the coeval
254 igneous rocks in the Jiangnan Orogen in South China as mentioned before (Fig.4; Yao
255 et al., 2019). Taken together, it is obvious that the 0.83-0.70 Ga zircons of the
256 Ordovician samples could not originate mainly from the erosion of the Panxi-Hannan
257 arc magmatic rocks in the western Yangtze Terrane. In contrast, it is possible that most
258 of the 0.83-0.70 Ga zircons in the Ordovician sediments in the Eastern Yidun
259 subterrane were derived from the Jiangnan Orogen. Concerning the 1.00-0.90 Ga and

260 0.65-0.50 Ga detrital zircons, they were impossibly sourced from the coeval igneous
261 rocks in the interior of South China due to the absence of synchronous magmatic
262 rocks within South China. Therefore, they could be exotic by a long distance transport
263 or recycled from the old strata in South China (Cawood et al., 2018), which are
264 consistent with the subrounded and rounded attributes of these detrital zircons
265 (Fig.S1). Indeed, the Ordovician sediments in the Eastern Yidun subterrane share a
266 similar age spectrum and zircon Hf isotopic compositions to the Cambrian unit in the
267 western Yangtze Terrane (Chen et al., 2021), indicating that the former could be
268 primarily derived from the recycling of the latter, although their ultimate sources
269 include the Eastern Ghats-Rayner Complex and the Kuunga Orogen located in the
270 eastern India region, and the Jiangnan Orogen in South China.

271

272 ***5.2. Tectonic link between South China and India***

273 Two contrasting reconstruction models have been proposed for the
274 paleogeographic position of South China in Rodinia: an internal location within the
275 Rodinia supercontinent versus an external setting along the margin of the Rodinia
276 supercontinent (e.g., Cawood et al., 2018; Li et al., 1999, and references therein; Zhao
277 & Cawood, 1999). For the internal model, South China was located between the
278 Laurentia and Australia blocks (e.g., Li et al., 1999; Li et al., 2002). In the peripheral
279 model, South China was attached to India in the Early to Mid-Neoproterozoic (e.g.,
280 Cawood et al., 2018; Zhao et al., 2018b).

281 In fact, increasing lines of evidence including magmatic, paleomagnetic, and
282 sedimentary data (e.g., [Cawood et al., 2018](#); [Chen et al., 2021](#); [Gregory et al., 2009](#);
283 [Wang et al., 2017a, 2021](#); [Yang et al., 2004](#); [Yao et al., 2014](#); [Zhao et al., 2018b](#)), have
284 demonstrated that South China could be located to the periphery of Rodinia rather
285 than an intra-cratonic position during Neoproterozoic time. Nonetheless, the
286 spatio-temporal evolution of South China within these peripheral models from
287 Rodinia to Gondwana by different researchers is also different. For example, based on
288 the paleomagnetic studies on the Middle Cambrian sediments from the western
289 Yangtze Terrane, [Yang et al. \(2004\)](#) proposed that South China was connected with
290 NW Australia during latest Proterozoic and Early Paleozoic times, until its breakup
291 from Australia in the Middle Devonian. In contrast, by comparison of detrital zircon
292 age spectra between the Gondwana-derived blocks/terranes, [Yao et al. \(2014\)](#)
293 suggested that the Cathaysia side of South China was closely linked with the northern
294 margin of India (the Himalaya region) by the Ediacaran-Cambrian collision between
295 South China and India and persisted until the opening of the Paleo-Tethys Ocean
296 during Devonian time. In recent years, by comparisons of magmatism, sedimentation,
297 bio-stratigraphic affinity and paleomagnetic pole of South China with India and
298 Australia, some researchers concluded that South China was most likely close to
299 northern India during Neoproterozoic and even Early Cambrian times but was
300 progressively separating from the latter, and rotating and migrating along the
301 Gondwana margin toward northeastern India and NW Australia during latest
302 Ediacaran or Early Cambrian time (e.g., [Chen et al., 2021](#); [Jiang et al., 2003](#); [Wang et](#)

303 al., 2021).

304 However, keeping a consistently main age group from the Tonian to Cambrian
305 strata on the Cathaysia Terrane and on the western Yangtze Terrane although their
306 main age groups are different, such as ca. 960 Ma for the former and ca. 800 Ma for
307 the latter, respectively (Fig. 5; Wang et al., 2021; Yao et al., 2014), indicate that their
308 detrital provenances did not change with time. In other words, they each shared a
309 common source from the Tonian to Cambrian although the provenance is different
310 between them. This, in turn, hints that the tectonic setting for the Tonian to Cambrian
311 sedimentation in these two terranes did not change. Accordingly, it is unlikely that the
312 Yangtze Terrane commenced to rift from northwestern India since the late Tonian and
313 South China was migrating towards NW Australia. Moreover, the absence of
314 diagnostic ca. 1170 Ma age group of NW Australia in the Tonian to Early Paleozoic
315 strata in the Cathaysia Terrane (Fig. 5; e.g., Wang et al., 2010; Yao et al., 2014) also
316 argues against a close proximity to NW Australia during Tonian to Early Paleozoic
317 time. By contrast, the presence of a predominant age population of detrital zircons at
318 ca. 960 Ma from the Tonian to Cambrian strata in the Cathaysia Terrane (Fig. 5; e.g.,
319 Wang et al., 2010; Yao et al., 2014), suggests that a common northern Indian (the
320 Tethyan sequences) detrital provenance had continuously provided the detritus input
321 into the Cathaysia Terrane from the Tonian to Cambrian. In fact, the similarities in
322 facies assemblages of the late Neoproterozoic-Early Cambrian sedimentary rocks
323 between South China and India also lend strong support to this proposition. For
324 example, the Yangtze Terrane of South China and NW India share similar late Tonian

325 rift-related siliciclastic-volcanic successions, Cryogenian glaciogenic diamictite
326 successions, Ediacaran carbonate successions, Early Cambrian phosphorite and clastic
327 successions (Jiang et al., 2003). Correspondingly, the Cathaysia Terrane and eastern
328 India region contain similar Tonian siliciclastics, Cryogenian sandstones and
329 diamictites, Ediacaran-Cambrian siliciclastics (Wang & Li, 2003; Wang et al., 2021).
330 As a consequence, we propose that South China should keep a close linkage with
331 India and form the South China-India Duo at least during late Tonian to Cambrian
332 time as the connection model proposed by Cawood et al. (2018) and Zhao et al.
333 (2018b). It was finally separated from Indian Gondwana likely after the Early
334 Cambrian due to the opening of Proto-Tethys Ocean (ca. 510 Ma) rather than
335 Paleo-Tethys Ocean after the Devonian (also see discussion in Section 5.4).

336

337 *5.3. Double late Neoproterozoic rift systems developed in the South China-India*

338 *Duo*

339 Increasing lines of evidence, such as comparable Neoproterozoic rift-related
340 magmatism and sedimentation between the Nanhua tectonic zone in South China and
341 the Aravalli-Delhi fold belt in NW India, illustrate the development of a
342 Neoproterozoic intracontinental linear rift basin in the interior of the South
343 China-India Duo (Fig. 6; Wang & Li, 2003; Wang et al., 2017a; Zhao et al., 2018b,
344 and references therein). For example, from a sedimentation perspective, some coeval
345 extension-related basins with similar lithological assemblages and sedimentary
346 sequences had developed in the Sindreh and Punagarh basins along the western

347 margin of the Aravalli-Dehli fold belt in NW India (Jiang et al., 2003; Zhao et al.,
348 2018b, and references therein), the unnamed basin in the Lesser Himalaya north of
349 the Aravalli-Dehli fold belt (i.e., the Jaunsar-Simla and Blaini sequences; Jiang et al.,
350 2003; Zhao et al., 2018b, and references therein), and the Nanhua basin in South
351 China (Wang & Li, 2003; Zhao et al., 2018b). In addition, the late Tonian-Ediacaran
352 sedimentary sequences in the Nanhua and Aravalli-Dehli basins share similar detrital
353 zircon age patterns and overlapping $\epsilon_{\text{Hf}}(t)$ values (Fig. 5), which also favors the idea
354 of depositional continuity among the Nanhua-Aravalli-Dehli basin at that time.
355 Besides, similar Neoproterozoic rift-related magmatism, including the bimodal
356 magmatic rocks and A-type granites that are generally produced in extension-related
357 regimes, has been identified in the Malani Igneous Suite located to the western margin
358 of the NE-trending Aravalli-Dehli fold belt of NW India (e.g., Wang et al., 2017a;
359 Zhao et al., 2018b; and references therein) and the Nanhua basin in South China (e.g.,
360 Deng et al., 2016; Li et al., 2021; Wang & Li, 2003). More importantly, the
361 recognition of Late Neoproterozoic lower $\delta^{18}\text{O}$ magmatic zircons ($<5\text{‰}$) than that of
362 mantle values ($5.3 \pm 0.6\text{‰}$; Valley et al., 1998) in these two aforementioned belts (Fig.
363 6; Li et al., 2021; Wang et al., 2017a; Zhang et al., 2020a; Zhao et al., 2018b; and
364 references therein), indicates the development of a synchronous rifting in NW India
365 and the interior of South China as pointed out by Zhao et al. (2018b).

366 In fact, an alternative Neoproterozoic extension-related tectonic zone had also
367 developed simultaneously along the northern and western margins of the Yangtze
368 Terrane of South China. For instance, the occurrence of some Neoproterozoic

369 extension-related igneous rocks on the western margin of the Yangtze Terrane,
370 including the Tiechuanshan (ca. 820 Ma) and Suxiong (ca. 800 Ma) bimodal volcanic
371 rocks, and the Daxiangling (ca. 816 Ma), and Tiechuanshan, Huangguan and
372 Mianning (780 Ma), and Panzhihua (750 Ma) A-type granites, and low- $\delta^{18}\text{O}$
373 magmatic rocks (Fig. 6; e.g., Li et al., 2002; Wu et al., 2020; and references therein),
374 suggests an extensional setting at that time. Although a mantle plume setting has been
375 invoked to account for such extension-related magmatism (Li et al., 2002; Wang et al.,
376 2007a), this scenario fails to explain the presence of more voluminous 820-770 Ma
377 magmatic rocks featured by typical arc geochemical signature in the Panxi-Hannan
378 region on the northern and western Yangtze Terrane (Zhao et al., 2011; Zhao et al.,
379 2018b; and references therein). In contrast, a prolonged subduction-related arc
380 environment as proposed by some authors (Cawood et al., 2018; Zhao et al., 2018b;
381 Zhou et al., 2006; and references therein) can have also developed at 820-770 Ma.
382 Moreover, the arc-like geochemical characteristics and high proportion of younger
383 detrital zircon age population (CA-DA<100 Ma in 30% of the zircon population; Fig.
384 7) of the Neoproterozoic metasedimentary samples from the Yidun Terrane also
385 indicated the deposition in a convergent setting basin (Cawood et al., 2012; Tian et al.,
386 2020). In this respect, a back-arc environment is likely a plausible interpretation for
387 the coexistence of arc- and extension-type magmatic rocks on the western and
388 northern margins of the Yangtze Terrane, as assumed recently by Luo et al. (2018).
389 However, such a model is incompatible with their magmatic pattern dominated by
390 arc-type magmatic rocks with some extension-related rocks in this region as

391 mentioned before (Cawood et al., 2018; Zhao et al., 2018b). In other words, these
392 Neoproterozoic arc-type magmatic rocks should represent the important component of
393 simultaneous continental arc. Moreover, considering that a huge thickness of
394 extension-related late Neoproterozoic volcanoclastic sediments (> 5 km) coexist with
395 synchronous magmatic rocks on the northern and western margins of the Yangtze
396 Terrane and the southeastern margin of the Ganzê and Yidun terranes (BGMRSP,
397 1984), we propose that an intra-arc rifting is the most feasible explanation for such a
398 coupling of magmatism and sedimentation. In fact, intra-arc rifting has been
399 established in different subduction zones, such as northeast Japan of west Pacific
400 (Nakajima, 2013), and the Anglona region of northwestern Sardinia, Italy (Sowerbutts,
401 2000). In particular, the magmatic association and sedimentary pattern on the northern
402 and western margins of the Yangtze Terrane are similar to those in the intra-arc rift
403 basin in the Anglona region of northwestern Sardinia, Italy (Sowerbutts, 2000).

404 As the important parts of the Neoproterozoic subduction system on the western
405 margin of Rodinia (e.g., Cawood et al., 2018; Wang et al., 2021; Zhao et al., 2018b),
406 the coexistence of coeval extension-related magmatic rocks and sedimentary basins
407 together with a large number of subduction-related arc-type igneous rocks in
408 Madagascar and Seychelles likewise indicates the development of an intra-arc rifting
409 at that time, resembling those on the western and northern margins of the Yangtze
410 Terrane as stated above. For instance, the recognition of some mafic-ultramafic
411 plutons with layered Fe-Ti-V oxide mineralization, A-type granitoids with a strongly
412 alkaline composition and bimodal magmatic suite in the Imorona-Itsindro Suite of

413 central Madagascar ([Archibald et al., 2017](#); [Nédélec et al., 2016](#); [Zhou et al., 2018a](#);
414 and references therein), coupled with the same extensional structural signature
415 between the ca. 790 Ma Imorona-Itsindro rocks and their country rocks ([Nédélec et al.,](#)
416 [2016](#), and references therein), has been recently interpreted as the products of
417 continental rifting by [Zhou et al. \(2018a\)](#). Furthermore, from a variation of isotopic
418 composition perspective, especially for zircon Hf and O isotopes of the 850-750 Ma
419 magmatic rocks in the central Madagascar, [Zhou et al. \(2018a\)](#) believed that
420 synchronous continental rifting had been involved in their petrogenesis. On the other
421 hand, these central Madagascar rocks are dominated by calc-alkaline series and
422 geochemically show an affinity to volcanic or continental arc magmatic rocks, most
423 researchers ascribed their generation to the results of prolonged Andean-like arc
424 magmatism ([Archibald et al., 2017](#); [Handke et al., 1999](#); [Kröner et al. 2000](#); [Tucker et](#)
425 [al. 1999b](#)). In Seychelles, the 810-700 Ma magmatic rocks also display the coupling
426 of a typical Andean-type arc and rift-type (low- $\delta^{18}\text{O}$ granites) geochemical signatures
427 (e.g., [Ashwal et al., 2002](#), and references therein). Taken together, we propose that a
428 late Neoproterozoic intra-arc rift system could have developed along the northern and
429 western margins of the Yangtze Terrane, through the Marwar Terrane of western
430 India, and then into Seychelles and Madagascar, although such lines of evidence from
431 western India are still absent so far ([Fig. 6](#)). Such an intra-arc rift system along the
432 western margin of the South China-India Duo is different from the contemporaneous
433 intracontinental one (the Nanhua-Aravalli-Delhi rift system) within it ([Fig. 6](#)).
434 Moreover, it can also account for the contradiction about the common presence of

435 coeval arc-type and extension-related magmatic rocks coupled with some
436 extension-related sedimentation in the same area.

437 The most plausible mechanism responsible for the development of such double
438 synchronous rift systems should be attributed to the rollback of subducting oceanic
439 slab beneath the South China-India Duo (Fig. 6), which would result in the
440 asthenospheric upwelling and subsequent lithospheric extension at that time. As the
441 old suture belts, the Jiangnan fold belt between the Yangtze and Cathaysia terranes in
442 South China (Zhao et al., 2011) and the Aravalli-Dehli fold belt between the Marwar
443 and Bundelkhand terranes in NW India (Zhao et al., 2018b) are the most ideal areas to
444 produce lithospheric extension. As a result, it is the most effective mechanism to
445 induce an intracontinental rifting. An alternative region apt to trigger lithospheric
446 extension is the continental arc, especially the intra-arc where arc magmatism
447 develops frequently and trans-lithospheric faults widely occur. Such a scenario can
448 also be an important mechanism for the fragmentation of some
449 micro-continents/terranes/blocks from a big continent by the intra-arc rifting.

450

451 ***5.4. Implication for breakup of South China from Gondwana***

452 Different researchers have proposed different breakup times for South China from
453 Gondwana. For example, earlier studies suggested the separating time from the Early
454 Cambrian to Silurian in light of the variation of biogeography and stratigraphy in
455 South China (Jiang et al., 2003, and references therein). Subsequently, considering the

456 opening of Paleo-Tethys Ocean between the South China and Indochina blocks, most
457 workers believed that South China had broken up from Gondwana in the Devonian
458 (e.g., [Cawood et al., 2013](#); [Chen et al., 2021](#); [Metcalf, 2013](#); [Wang et al., 2021](#)). The
459 critical evidence is the dating results of the remnant oceanic components, the oldest
460 plagiogranites of which at Shuanggou from the Jinshajiang-Ailaoshan Paleo-Tethys
461 suture yielded zircon U-Pb ages of ca. 383-376 Ma ([Jian et al., 2009](#)). More recently,
462 by comparison of the Neoproterozoic to Early Paleozoic detrital zircon age spectra of
463 South China with India and Australia, [Wang et al. \(2021\)](#) and [Chen et al. \(2021\)](#)
464 proposed the initial separation time of South China from NW India in the Cryogenian
465 and Early Cambrian, respectively. Moreover, based on the opening of Paleo-Tethys
466 Ocean, they both concluded that South China should have finally drifted away from
467 the northern margin of Australian Gondwana in the Devonian ([Chen et al., 2021](#);
468 [Wang et al., 2021](#)).

469 Regardless of how South China broke up from Gondwana, all the views ignore a
470 crucial fact that the Proto-Tethys Ocean between South China and other
471 Gondwana-derived blocks had also developed in the Early Paleozoic. The opening of
472 the Proto-Tethys Ocean should have ever led to the separation of South China from
473 northern Gondwana. For instance, the Early Paleozoic oceanic relics, including
474 477-460 Ma MORB-type clinopyroxenite, gabbro and amphibolite, and 519-502 Ma
475 plagiogranites in the Tam Ky-Phuoc Son suture of Vietnam ([Gardner et al., 2017](#);
476 [Nguyen et al., 2019](#), and references therein), indicate the presence of an Early
477 Paleozoic Ocean between the South China and Indochina blocks or South

478 China-northern Indochina and southern Indochina blocks (Faure et al., 2018; Nguyen
479 et al., 2019). On the other hand, another Proto-Tethys Ocean (518-438 Ma) between
480 the South Qiangtang-Baoshan and North Qiangtang-Indochina terranes has been also
481 documented in recent years (e.g., Hu et al., 2014; Wu, 2013). In particular, the
482 identification of the Cambrian ophiolites (ca. 517-490 Ma; Hu et al., 2014; Wu, 2013)
483 implies the development of a Tethys Ocean at least in the Middle Cambrian. In this
484 regard, it is suggested that the Indochina Block had rifted away from the northern
485 margin of Gondwana in the Middle Cambrian-Early Silurian interval. It is, in turn, the
486 most plausible to infer that South China had been ever separated from the northern
487 Gondwana at least from the Middle Cambrian to Early Silurian (Fig. 8; Liu et al.,
488 2020a).

489 Whether South China had been assembled together with northern Gondwana by
490 continent-continent collision similar to the collision between the South China and
491 Indochina blocks in the Late Silurian remains unknown. Although Zhang et al. (2014)
492 proposed a continent-continent collision time at 427-422 Ma based on the study of
493 high-pressure basic granulites in the Central Qiangtang of Tibet, the identification of
494 coeval (438 ± 11 Ma) oceanic cumulate gabbro in the same ophiolitic complex belt of
495 central Qiangtang likely indicates that the Early Paleozoic Proto-Tethys Ocean had
496 not been closed (Wu, 2013). In fact, no age-equivalent collision-related records have
497 been discovered so far in the Changning-Menglian ophiolite belt that represents the
498 southern continuation of the central Qiangtang Proto-Tethys Ocean. More importantly,
499 the identification of the Early and Late Paleozoic oceanic OIB-type mafic rocks that

500 had commonly experienced a same Late Triassic ultrahigh-pressure metamorphism
501 (Fan et al., 2015), indicates that the Proto-Tethys Ocean could have developed
502 persistently from the Early Paleozoic to the end of the Paleozoic (Liu et al., 2020a,
503 and references therein). Therefore, it is most likely that the Central Qiangtang
504 high-pressure granulites within Tibet (Zhang et al., 2014) could be the products of
505 Early Paleozoic arc-continent collision during the tectonic evolution of a single Proto-
506 and Paleo-Tethys Ocean. Combing with all data (Chen et al., 2021, and references
507 therein), we propose that the South China and Indochina blocks were separated from
508 Indian Gondwana after the Early Cambrian and were not welded with Gondwana
509 again, although they were likely amalgamated together during Late Silurian time
510 (Faure et al., 2018; Nguyen et al., 2019) until the opening of the Paleo-Tethys Ocean
511 between them (Jian et al., 2009).

512

513 **6. Conclusions**

514 Our new zircon U-Pb dating and Hf isotope analysis for the Neoproterozoic-
515 Early Paleozoic (meta-) sedimentary sequences from the Eastern Yidun subterrane
516 that belongs to part of the Yangtze Terrane of South China, coupled with a detailed
517 compilation of big data published from South China, India and some blocks/terranes
518 separated from them, can draw the following conclusions:

519 (1) The Neoproterozoic sediments in the Eastern Yidun subterrane were sourced
520 mainly from the Panxi-Hannan magmatic arc on the northern and western margins of

521 the Yangtze Terrane while the Ordovician sequences were recycled from the
522 Cambrian strata in the western Yangtze Terrane.

523 (2) South China kept a connection with India and formed the South China-India Duo
524 located at northwestern margin of Rodinia during late Tonian (ca. 800 Ma) to Early
525 Cambrian time.

526 (3) Double late Neoproterozoic rift systems had developed in the South China-India
527 Duo owing to the rollback of subducting oceanic slab beneath it, including an
528 intra-arc rift along the northern and western margins of the Yangtze Terrane, through
529 the Marwar Terrane of western India, and then into the Seychelles and Madagascar,
530 and another coeval intracontinental one (the Nanhua-Aravalli-Delhi rift) separating
531 the Yangtze-Marwar from Cathaysia-Bundelkhand terranes within the interior of the
532 South China-India Duo.

533 (4) South China was finally separated from northern India during Middle
534 Cambrian-Ordovician time due to the opening of the Proto-Tethys Ocean (ca. 510 Ma)
535 but was not welded with Gondwana again.

536

537 **Acknowledgements**

538 This work was jointly supported by the National Second Expedition to the
539 Tibetan Plateau (2019QZKK0702) and National Natural Science Foundation of China
540 (92055207, 42072263, 41490613, 41672058). This is a contribution from the
541 Guangzhou Institute of Geochemistry, Chinese Academy of Sciences (GIG, CAS; No.
542 xxx). All data of this manuscript will be available at the Mendelay Data repository
543 (DOI: 10.17632/bs75p9fx6h.1).

544 **References**

- 545 Ao, W. H., Zhao, Y., Zhang, Y. K., Zhai, M. G., Zhang, H., Zhang, R. Y., Wang, Q., &
546 Sun, Y., 2019. The neoproterozoic magmatism in the northern margin of the
547 yangtze block: insights from Neoproterozoic (950-706 Ma) gabbroic-granitoid
548 rocks of the Hannan complex. *Precambrian Research*, 333, 105442. DOI:
549 10.1016/j.precamres.2019.105442
- 550 Armistead, S. E., Collins, A. S., Merdith, A. S., Payne, J. L., Cox, G. M., Foden, J. D.,
551 Razakamanana, T., De Waele, B., 2019. Evolving Marginal Terranes During
552 Neoproterozoic Supercontinent Reorganization: Constraints From the Bemarivo
553 Domain in Northern Madagascar. *Tectonics*, 38(6), 2019-2035. DOI:
554 10.1029/2018TC005384
- 555 Ashwal, L. D., Demaiffe, D., Torsvik, T. H., 2002. Petrogenesis of Neoproterozoic
556 granitoids and related rocks from the Seychelles: the case for an Andean-type arc
557 origin. *Journal of Petrology*, 43(1), 45-83. DOI: 10.1093/petrology/43.1.45
- 558 Bureau of Geology and Mineral Resources of Sichuan Province (BGMRS), 1980.
559 *The Geological map of the People's Republic of China, Yidun Regional (scale 1:*
560 *200,000)*. (Map H-47-16). Sichuan: BGMRS. (in Chinese)
- 561 Bureau of Geology and Mineral Resources of Sichuan Province (BGMRS), 1984.
562 *The Geological map of the People's Republic of China, Gongling Regional (scale 1:*
563 *200,000)*. (Map H-47-35). Sichuan: BGMRS. (in Chinese)
- 564 Cawood, P. A. & Buchan, C., 2007. Linking accretionary orogenesis with
565 supercontinent assembly. *Earth Science Reviews*, 82(3-4), 217-256. DOI:
566 10.1016/j.earscirev.2007.03.003
- 567 Cawood, P. A., Hawkesworth, C., Dhuime, B., 2012. Detrital zircon record and
568 tectonic setting. *Geology*, 40, 875-878. DOI: 10.1130/G32945.1
- 569 Cawood, P. A., Wang, Y. J., Xu, Y. J., Zhao, G. C., 2013. Locating South China in
570 Rodinia and Gondwana: a fragment of greater India lithosphere? *Geology*, 41 (8),
571 903-906. DOI: 10.1130/G34395.1
- 572 Cawood, P. A., Zhao, G. C., Yao, J. L., Wang, W., Xu, Y. J., Wang, Y. J., 2018.

573 Reconstructing South China in Phanerozoic and Precambrian supercontinents.
574 *Earth Science Reviews*, 186, 173-194. DOI: 10.1016/j.earscirev.2017.06.001

575 Chen, Q., Sun, M., Long, X., Zhao, G., & Yuan, C., 2016. U-Pb ages and Hf isotopic
576 record of zircons from the late Neoproterozoic and Silurian-Devonian sedimentary
577 rocks of the western Yangtze block: implications for its tectonic evolution and
578 continental affinity. *Gondwana Research*, 184-199. DOI: 10.1016/j.gr.2015.01.009

579 Chen, Q., Sun, M., Long, X., Zhao, G., Wang, J., Yu, Y., & Yuan, C., 2018.
580 Provenance study for the Paleozoic sedimentary rocks from the west Yangtze Block:
581 constraint on possible link of South China to the Gondwana supercontinent
582 reconstruction. *Precambrian Research*, 309, 271-289.
583 <https://doi.org/10.1016/j.precamres.2017.01.022>

584 Chen, Q., Zhao, G., Sun, M., 2021. Protracted northward drifting of South China
585 during the assembly of Gondwana: Constraints from the spatial-temporal
586 provenance comparison of Neoproterozoic-Cambrian strata. *Geological Society of
587 America Bulletin*, 1-17. <https://doi.org/10.1130/B35791.1>

588 Cui, X., Zhu, W. B., Fitzsimons, I. C. W., He, J. W., Lu, Y. Z., Wang, X., Ge, R. F.,
589 Zheng, B. H. & Wu, X., 2015. U-Pb age and Hf isotope composition of detrital
590 zircons from Neoproterozoic sedimentary units in southern Anhui Province, South
591 China: implications for the provenance, tectonic evolution and glacial history of the
592 eastern Jiangnan Orogen. *Precambrian Research*, 271, 65-82.
593 <https://doi.org/10.1016/j.precamres.2015.10.004>

594 DeCelles, P. G., Gehrels, G. E., Quade, J., Lareau, B. & Spurlin, M., 2000. Tectonic
595 implications of U-Pb zircon ages of the Himalayan orogenic belt in Nepal. *Science*,
596 288(5465), 497-499. DOI: 10.1126/science.288.5465.497

597 Deng, Q., Wang, Z., Jian, W., Hu, Z., Fei, Y., 2016. 800~780 Ma continental rift
598 magmatism in the eastern part of the Jiangnan orogen: implications from ~790 Ma
599 aluminous A-type granites in Zhejiang-Anhui-Jiangxi border area. *Geological
600 Bulletin of China*, 35(11), 1855-1868.

601 Dickinson, W. R., Gehrels, G. E., 2009. Use of U-Pb ages of detrital zircons to infer
602 maximum depositional ages of strata: a test against a Colorado Plateau Mesozoic

603 database. *Earth and Planetary Science Letters*, 288(1-2), 115-125.
604 <https://doi.org/10.1016/j.epsl.2009.09.013>

605 Fan, W. M., Wang, Y. J., Zhang, Y. H., Zhang, Y. Z., Jourdan, F., & Liu, H.C., 2015.
606 Paleotethyan subduction process revealed from Triassic blueschists in the Lancang
607 tectonic belt of Southwest China. *Tectonophysics*, 662, 95-108.
608 <https://doi.org/10.1016/j.tecto.2014.12.021>

609 Faure, M., Nguyen, V.V., Hoai, L.T.T., Lepvrier, C., 2018. Early Paleozoic or
610 Early-Middle Triassic collision between the South China and Indochina Blocks: the
611 controversy resolved? Structural insights from the Kon Tum massif (Central
612 Vietnam). *Journal of Asian Earth Sciences*, 166, 162-180.
613 <https://doi.org/10.1016/j.jseaes.2018.07.015>.

614 Gardner, C. J., Graham, I. T., Belousova, E., Booth, G. W., & Greig, A., 2017.
615 Evidence for Ordovician subduction-related magmatism in the Truong Son terrane,
616 SE Laos: implications for Gondwana evolution and porphyry Cu exploration
617 potential in SE Asia. *Gondwana Research*, 44, 139-156.
618 DOI:10.1016/j.gr.2016.11.003

619 Gehrels, G. E., Decelles, P. G., Ojha, T. P., & Upreti, B. N., 2006. Geologic and U-Pb
620 geochronologic evidence for early paleozoic tectonism in the Dadeldhura thrust
621 sheet, far-west Nepal Himalaya. *Journal of Asian Earth Sciences*, 28(4-6), 385-408.
622 <https://doi.org/10.1016/j.jseaes.2005.09.012>

623 Gehrels, G., Kapp, P., Decelles, P., Pullen, A., Blakey, R., Weislogel, A., et al., 2011.
624 Detrital zircon geochronology of pre-tertiary strata in the Tibetan-Himalayan
625 orogen. *Tectonics*, 30(5), 1-27. <https://doi.org/10.1029/2011TC002868>

626 Gregory, L. C., Meert, J. G., Bingen, B., Pandit, M. K., & Torsvik, T. H., 2009.
627 Paleomagnetism and geochronology of the Mlani igneous suite, northwest India:
628 implications for the configuration of Rodinia and the assembly of Gondwana.
629 *Precambrian Research*, 170(1-2), 13-26. DOI: 10.1016/j.precamres.2008.11.004

630 Haines, P. W., Kirkland, C. L., Wingate, M. T. D., Allen, H., Belousova, E. A., &
631 Gréau, Y., 2016. Tracking sediment dispersal during orogenesis: A zircon age and
632 Hf isotope study from the western Amadeus Basin, Australia. *Gondwana Research*,

633 37, 324-347. <https://doi.org/10.1016/j.gr.2015.08.011>

634 Handke, M. J., Tucker, R. D., & Ashwal, L. D., 1999. Neoproterozoic continental arc
635 magmatism in west-central Madagascar. *Geology*, 27(4), 351-354.
636 [https://doi.org/10.1130/0091-7613\(1999\)027<0351:NCAMIW>2.3.CO;2](https://doi.org/10.1130/0091-7613(1999)027<0351:NCAMIW>2.3.CO;2)

637 Harris, C., & Ashwal, L. D., 2002. The origin of low delta O-18 granites and related
638 rocks from the Seychelles. *Contributions to Mineralogy and Petrology*, 143(3),
639 366-376. DOI: 10.1007/s00410-002-0349-6

640 He, Y. Y., Niu, Z. J., Yao, H. Z., Song, F., & Yang, W. Q., 2020. Provenance and
641 tectonic setting of the Ordovician sedimentary succession at the southeastern
642 margin of the Yangtze Block, South China: Implications for paleotopographic
643 evolution of northeastern Gondwana. *Journal of Asian Earth Sciences*, 202,
644 104532. <https://doi.org/10.1016/j.jseaes.2020.104532>

645 Hofmann, M. H., Li, X. H., Chen, J., MacKenzie, L. A., & Hinman, N. W., 2016.
646 Provenance and temporal constraints of the early Cambrian Maotianshan shale,
647 Yunnan province, China. *Gondwana Research*, 37, 348-361. DOI:
648 10.1016/j.gr.2015.08.015

649 Hofmann, M., Linnemann, U., Rai, V., Becker, S., Gartner, A. & Sagawe, A., 2011.
650 The India and South China cratons at the margin of Rodinia-synchronous
651 Neoproterozoic magmatism revealed by LA-ICP-MS zircon analyses. *Lithos*,
652 123(1-4), 176-187. <https://doi.org/10.1016/j.lithos.2011.01.012>

653 Hu, P. Y., Li, C., Wu, Y. W., Xie, C. M., Wang, M., Zhang, H. Y., & Li, J., 2014. The
654 Silurian Tethyan Ocean in central Qiangtang, northern Tibet: Constraints from
655 zircon U-Pb ages of plagiogranites within the Taoxinghu ophiolite. *Geological*
656 *Bulletin of China*, 33(11), 1651-1661.

657 Huang, D. L., Wang, X. L., Xia, X. P., Wan, Y. S., Zhang, F. F., Li, J. Y., & Du, D. H.,
658 2018. Neoproterozoic Low-delta O-18 Zircons Revisited: Implications for Rodinia
659 Configuration. *Geophysical Research Letters*, 46(2), 678-688. DOI:
660 10.1029/2018GL081117

661 Hughes, N. C., Myrow, P. M., Ghazi, S., McKenzie, N. R., Stockli, D. F., DiPietro, J.
662 A., 2019. Cambrian geology of the Salt Range of Pakistan: Linking the Himalayan

663 margin to the Indian craton. *Geological Society of America Bulletin*, 131(7-8),
664 1095-1114. DOI: 10.1130/B35092.1

665 Hughes, N. C., Myrow, P. M., McKenzie, N. R., Harper, D. A. T., Bhargava, O. N.,
666 Tangri, S. K., Ghalley, K. S., and Fanning, C. M., 2011. Cambrian rocks and faunas
667 of the Wachi La, Black Mountains, Bhutan. *Geological Magazine*, 148(3), 351-379.
668 DOI: 10.1017/S0016756810000750

669 Jian, P., Liu, D. Y., Kröner, A., Zhang, Q., Wang, Y. Z., Sun, X. M., & Zhang, W.,
670 2009. Devonian to Permian plate tectonic cycle of the Paleo-Tethys Orogen in
671 southwest China: Insights from zircon ages of ophiolites, arc/back-arc assemblages
672 and within-plate igneous rocks and generation of the Emeishan CFB province.
673 *Lithos*, 113: 767-784. <https://doi.org/10.1016/j.lithos.2009.04.006>

674 Jiang, G. Q., Sohl, L. E., & Christie-Blick, N., 2003. Neoproterozoic stratigraphic
675 comparison of the Lesser Himalaya (India) and Yangtze block (South China):
676 Paleogeographic implications. *Geology*, 31(10), 917-920. DOI: 10.1130/G19790.1

677 Jiang, X. W., Zou, H., Bagas, L., Chen, H. F., Liu, H., Li, Y., Li, M., & Li, D., 2020.
678 The Mojiawan I-type granite of the Kangding Complex in the western Yangtze
679 Block: new constraint on the Neoproterozoic magmatism and tectonic evolution of
680 South China. *International Geology Review*, 1-21. DOI:
681 10.1080/00206814.2020.1833254

682 Johnson, E. L., Phillips, G., & Allen, C. M., 2016. Ediacaran-Cambrian basin
683 evolution in the Koonenberry Belt (eastern Australia): implications for the
684 geodynamics of the Delamerian Orogen. *Gondwana Research*, 37, 266-284. DOI:
685 10.1016/j.gr.2016.04.010

686 Keemana, J., Turnera, S., Haines, W. P., Belousova, E., Ireland, T., Brouwer, P., Foden,
687 J., & Wörner, G., 2020. New U-Pb, Hf and O isotope constraints on the provenance
688 of sediments from the Adelaide Rift Complex-Documenting the key
689 Neoproterozoic to early Cambrian succession. *Gondwana Research*, 83, 248-278.
690 <https://doi.org/10.1016/j.gr.2020.02.005>

691 Kröner, A., Hegner, E., Collins, A. S., Windley, B. F., Brewer, T. S., Razakamanana,
692 T., & Pidgeon, R. T., 2000. Age and magmatic history of the Antananarivo Block,

693 central Madagascar, as derived from zircon geochronology and Nd isotopic
694 systematics. *American Journal of Science*, 300(4), 251-288. DOI:
695 <https://doi.org/10.2475/ajs.300.4.251>

696 Lan, Z. W., Zhang, S. J., Li, X. H., Pandey, S. K., Sharma, M., Shukla, Y., Ahmad, S.,
697 Sarkar, S. & Zhai, M. G., 2020. Towards resolving the 'jigsaw puzzle' and
698 age-fossil inconsistency within East Gondwana. *Precambrian Research*, 345, 1-18.
699 <https://doi.org/10.1016/j.precamres.2020.105775>

700 Li, J. Y., Wang, X. L., & Gu, Z. D., 2018. Petrogenesis of the Jiaoziding granitoids
701 and associated basaltic porphyries: Implications for extensive early Neoproterozoic
702 arc magmatism in western Yangtze Block. *Lithos*, 296, 547-562. DOI:
703 [10.1016/j.lithos.2017.11.034](https://doi.org/10.1016/j.lithos.2017.11.034)

704 Li, X. H., Li, W. X., Li, Z. X., & Liu, Y., 2008. 850-790 Ma bimodal volcanic and
705 intrusive rocks in northern Zhejiang, South China: a major episode of continental
706 rift magmatism during the breakup of Rodinia. *Lithos*, 102(1-2), 341-357. DOI:
707 [10.1016/j.lithos.2007.04.007](https://doi.org/10.1016/j.lithos.2007.04.007)

708 Li, X. H., Li, Z. X., Zhou, H. W., Liu, Y., & Kinny, P. D., 2002. U-Pb zircon
709 geochronology, geochemistry and Nd isotopic study of Neoproterozoic bimodal
710 volcanic rocks in the Kangdian Rift of South China: Implications for the initial
711 rifting of Rodinia. *Precambrian Research*, 113 (1-2), 135-154. DOI:
712 [10.1016/S0301-9268\(01\)00207-8](https://doi.org/10.1016/S0301-9268(01)00207-8)

713 Li, Y. X., Yin, C. Q., Lin, S. F., Zhang, J., Gao, P., Qian, J. H., Xia, Y. F. & Liu, J. N.,
714 2021. Geochronology and geochemistry of bimodal volcanic rocks from the
715 western Jiangnan Orogenic Belt: Petrogenesis, source nature and tectonic
716 implication. *Precambrian Research*, 359, 106218.
717 <https://doi.org/10.1016/j.precamres.2021.106218>

718 Li, Z. X., Li, X. H., Kinny, P. D., & Wang, J., 1999. The breakup of Rodinia: did it
719 start with a mantle plume beneath South China? *Earth and Planetary Science*
720 *Letters*, 173(3), 171-181. [https://doi.org/10.1016/S0012-821X\(99\)00240-X](https://doi.org/10.1016/S0012-821X(99)00240-X)

721 Liu, B. B., Peng, T. P., Fan, W. M., Zhao, G. C., Gao, J. F., Dong, X. H., & Peng, B.
722 X., 2020. Tectonic Evolution and Paleoposition of the Baoshan and Lincang Blocks

723 of West Yunnan During the Paleozoic. *Tectonics*, 39(10), e2019TC006028.

724 Liu, H., Wang, Z. J., Deng, Q., Du, Q. D., & Yang, F., 2019a. Constraints on the onset
725 age of the Sturtian glaciation from the Southeast Yangtze Block, South China.
726 *International Geology Review*, 61(15), 1876-1886.
727 <https://doi.org/10.1080/00206814.2019.1566787>

728 Liu, S. L., Cui, X. Z., Wang, C. L., Ren, G. M., Wang, P., Pang, W. H., & Ren, F.,
729 2020. New Sedimentological and Geochronological Evidence for
730 Mid-Neoproterozoic Rifting in Western Yangtze Block, South China. *Earth Science*,
731 45(8), 3082-3093 (In Chinese with English abstract). DOI: 10.3799/dqkx.2020.145

732 Liu, X. J., Xu, Z. Q., Zhen, Y. L. and Ma, Z. L., 2019c. Characteristics of detrital
733 zircon U-Pb geochronology and Hf isotopics from Liwu Group within the
734 Changqiang dome on the southeastern margin of Songpan-Ganzi terrane and its
735 tectonic implications. *Acta Petrologica Sinica*, 35(6): 169-1716. (In Chinese with
736 English abstract). DOI: 10.18654/1000-0569 /2019. 06. 05

737 Liu, Y. S., Hu, Z. C., Zong, K. Q., Gao, C. G., Gao, S., Xu, J., & Chen, H. H., 2010.
738 Reappraisal and refinement of zircon U-Pb isotope and trace element analyses
739 by LA-ICP-MS. *Chinese Science Bulletin*, 55(15), 1535-1546. DOI:
740 10.1007/s1143-010-3052-4

741 Liu, Y., Yang, K. G., Polat, A., & Ma, X., 2019b. Reconstruction of the Cryogenian
742 palaeogeography in the Yangtze Domain: constraints from detrital age patterns.
743 *Geological Magazine*, 56(7), 1247-1264. DOI: 10.1017/S0016756818000535

744 Long, S., Mcquarrie, N., Tobgay, T., Rose, C., Gehrels, G., & Grujic, D., 2011.
745 Tectonostratigraphy of the lesser Himalaya of Bhutan: implications for the
746 along-strike stratigraphic continuity of the northern Indian margin. *Geological*
747 *Society of America Bulletin*, 123(7-8), 1406-1426. DOI: 10.1130/B30202.1

748 Ludwig, K. R., 2003. User's manual for Isoplot 3.00: A geochronological toolkit for
749 Microsoft Excel. Berkeley Calif: Berkeley Geochronology Center.

750 Luo, B. J., Liu, R., Zhang, H. F., Zhao, J. H., Yang, H., Xu, W. C., Guo, L., Zhang, L.
751 Q., Tao, L., Pan, F. B., Wang, W., Gao, Z. & Shao, H., 2018. Neoproterozoic
752 continental back-arc rift development in the Northwestern Yangtze Block: Evidence

753 from the Hannan intrusive magmatism. *Gondwana Research*, 59, 27-42. DOI:
754 10.1016/j.gr.2018.03.012

755 Luo, L., Zeng, L. B., Wang, K., Yu, X.X., Li, Y.H., Zhu, C.X. & Liu, S. N., 2020.
756 Provenance investigation for the Cambrian-Ordovician strata from the northern
757 margin of the western Yangtze Block: implications for locating the South China
758 Block in Gondwana. *Geological Magazine*, 157(4), 551-572.
759 <https://doi.org/10.1017/S0016756819001110>

760 Ma, X., Yang, K. G., & Polat, A., 2019. U-Pb ages and Hf isotopes of detrital zircons
761 from pre-Devonian sequences along the southeast Yangtze: a link to the final
762 assembly of East Gondwana. *Geological Magazine*, 156(6), 950-968. DOI:
763 10.1017/S0016756818000511

764 Malone S. J., Meert, J. G., Banerjee, D. M., Pandit, M. K., Tamrat, E., Kamenov, G.
765 D., Pradhan, V. R. & Sohl, L. E., 2008. Paleomagnetism and detrital zircon
766 geochronology of the upper Vindhyan Sequence, Son Valley and Rajasthan, India:
767 A ca. 1000 Ma Closure age for the Purana Basins. *Precambrian Research*, 164(3-4),
768 137-159. <https://doi.org/10.1016/j.precamres.2008.04.004>

769 McKenzie, N. R., Hughes, N. C., Myrow, P. M., Xiao, S., & Sharma, M., 2011.
770 Correlation of Precambrian-Cambrian sedimentary successions across northern
771 India and the utility of isotopic signatures of Himalayan lithotectonic zones. *Earth
772 and Planetary Science Letters*, 312(3-4), 471-483. DOI: 10.1016/j.epsl.2011.10.027

773 McKenzie, N.C., Hughes, P. M., Myrow, P. M., Banerjee, D. M., Deb, M., &
774 Planavsky N. J., 2013. New age constraints for the Proterozoic Aravalli-Delhi
775 successions of India and their implications. *Precambrian Research*, 238, 120-128.
776 <https://doi.org/10.1016/j.precamres.2013.10.006>

777 Mcquarrie, N., Long, S. P., Tobgay, T., Nesbit, J. N., Gehrels, G., & Ducea, M. N.,
778 2013. Documenting basin scale, geometry and provenance through detrital
779 geochemical data: lessons from the Neoproterozoic to Ordovician lesser, greater,
780 and Tethyan Himalayan strata of Bhutan. *Gondwana Research*, 23(4), 1491-1510.
781 <https://doi.org/10.1016/j.gr.2012.09.002>

782 Metcalfe, I., 2013. Gondwana dispersion and Asian accretion: Tectonic and

783 palaeogeographic evolution of eastern Tethys. *Journal of Asian Earth Sciences*, 66,
784 1-33. <https://doi.org/10.1016/j.jseaes.2012.12.020>

785 Mukherjee, P. K., Jain, A. K., Singhal, S., Singha, N. B., Singh, S., Kumud, K., Seth,
786 P. & Patel, R. C., 2019. U-Pb zircon ages and Sm-Nd isotopic characteristics of the
787 lesser and great Himalayan sequences, Uttarakhand Himalaya, and their regional
788 tectonic implications. *Gondwana Research*, 75, 282-297.
789 <https://doi.org/10.1016/j.gr.2019.06.001>

790 Mulder, J. A., Everard, J. L., Cumming, G., Meffre, S., Bottrill, R. S., Merdith, A. S.,
791 Halpine, J. A., McNeill, A. W., & Cawood, P. A., 2020. Neoproterozoic opening of
792 the Pacific Ocean recorded by multi-stage rifting in Tasmania, Australia. *Earth*
793 *Science Reviews*, 201, 1-29. <https://doi.org/10.1016/j.earscirev.2019.103041>

794 Myrow, P. M., Hughes, N. C., Goodge, J. W., Fanning, C. M., Williams, I. S., & Peng,
795 S., 2010. Extraordinary transport and mixing of sediment across Himalayan central
796 Gondwana during the Cambrian-Ordovician. *Geological Society of America*
797 *Bulletin*, 122(9-10), 1660-1670. <https://doi.org/10.1130/B30123.1>

798 Nédélec, A., Paquette, J. L., Antonio, P., Paris, G., & Bouchez, J. L., 2016. A-type
799 stratoid granites of Madagascar revisited: Age, source and links with the breakup of
800 Rodinia. *Precambrian Research*, 280, 231-248.
801 <https://doi.org/10.1016/j.precamres.2016.04.013>

802 Nguyen, Q. M., Feng, Q., Zi, J. W., Zhao, T., Tran, H. T., Ngo, T. X., Tran, D. M. &
803 Nguyen, H. Q., 2019. Cambrian intra-oceanic arc trondhjemite and tonalite in the
804 Tam Ky-Phuoc Son Suture Zone, central Vietnam: Implications for the early
805 Paleozoic assembly of the Indochina Block. *Gondwana Research*, 70,
806 151-170. <https://doi.org/10.1016/j.gr.2019.01.002>

807 Peng, T. P., Zhao, G. C., Fan, W. M., Peng, B. X., & Mao, Y. S., 2014. Zircon
808 geochronology and Hf isotopes of Mesozoic intrusive rocks from the Yidun terrane,
809 Eastern Tibetan Plateau: petrogenesis and their bearings with Cu mineralization.
810 *Journal of Asian Earth Sciences*, 80, 18-33. DOI: 10.1016/j.jseaes.2013.10.028

811 Qasim, M., Ding, L., Khan, M. A., Umar, M., Jadoon, I. A. K., Haneef, M., Baral, U.,
812 Cai, F. L., Shah, A. & Yao, W., 2018. Late Neoproterozoic-early Palaeozoic

813 stratigraphic succession, western Himalaya, North Pakistan: detrital zircon
814 provenance and tectonic implications. *Geological Journal*, 53(9), 2258-2279. DOI:
815 10.1002/gj.3063

816 Qi, H., & Zhao, J. H., 2020b. Petrogenesis of the neoproterozoic low- $\delta^{18}\text{O}$ granitoids
817 at the western margin of the Yangtze block in South China. *Precambrian Research*,
818 351, 105953. <https://doi.org/10.1016/j.precamres.2020.105953>

819 Qi, L., Cawood, P. A., Xu, Y. J., Du, Y. S., Zhang, H. C. & Zhang, Z. K., 2020a.
820 Linking south china to north India from the late Tonian to Ediacaran: constraints
821 from the Cathaysia block. *Precambrian Research*, 350, 105898.
822 <https://doi.org/10.1016/j.precamres.2020.105898>

823 Qi, L., Xu, Y. J., Cawood, P. A., & Du, Y. S., 2018. Reconstructing Cryogenian to
824 Ediacaran successions and paleogeography of the South China Block. *Precambrian*
825 *Research*, 314, 452-467. <https://doi.org/10.1016/j.precamres.2018.07.003>

826 Shellnutt, J. G., Nguyen, D. T., & Lee, H. Y., 2020. Resolving the origin of the
827 Seychelles microcontinent: Insight from zircon geochronology and Hf isotopes.
828 *Precambrian Research*, 343, 105725. DOI: 10.1016/j.precamres.2020.105725

829 Sowerbutts, A., 2000. Sedimentation and volcanism linked to multiphase rifting in an
830 Oligo-Miocene intra-arc basin, Anglona, Sardinia. *Geological Magazine*, 137(4),
831 395-418. <https://doi.org/10.1017/S0016756800004246>

832 Sun, J. J., Shu, L. S., Santosh, M., & Wang, L. S., 2018. Precambrian crustal evolution
833 of the central Jiangnan Orogen (South China): Evidence from detrital zircon U-Pb
834 ages and Hf isotopic compositions of Neoproterozoic metasedimentary rocks.
835 *Precambrian Research*, 318, 1-24. DOI: 10.1016/j.precamres.2018.09.008

836 Sun, W. H., Zhou, M. F., Gao, J. F., Yang, Y. H., Zhao, X. F. & Zhao, J. H., 2009.
837 Detrital zircon U-Pb geochronological and Lu-Hf isotopic constraints on the
838 precambrian magmatic and crustal evolution of the western Yangtze block, SW
839 China. *Precambrian Research*, 172(1-2), 99-126. DOI:
840 10.1016/j.precamres.2009.03.010

841 Sun, W. H., Zhou, M. F., Yan, D. P., Li, J. W. & Ma, Y. X., 2008b. Provenance and
842 tectonic setting of the Neoproterozoic Yanbian group, western Yangtze block (SW

843 China). *Precambrian Research*, 167(1), 213-236.
844 <https://doi.org/10.1016/j.precamres.2008.08.001>

845 Tian, Z. D., Leng, C. B., & Zhang, X. C., 2020. Provenance and tectonic setting of the
846 neoproterozoic meta-sedimentary rocks at southeastern Tibetan plateau:
847 implications for the tectonic affinity of Yidun terrane. *Precambrian Research*, 344,
848 1-19. <https://doi.org/10.1016/j.precamres.2020.105736>

849 Turner, C. C., Meert, J. G., Pandit, M. K. & Kamenov, G. D., 2014. A detrital zircon
850 U-Pb and Hf isotopic transect across the Son Valley sector of the Vindhyan basin,
851 India: implications for basin evolution and paleogeography. *Gondwana Research*,
852 26(1), 348-364. <https://doi.org/10.1016/j.gr.2013.07.009>

853 Valley, J. W., Kinny, P. D., Schulze, D. J., & Spicuzza, M. J., 1998. Zircon megacrysts
854 from kimberlite: oxygen isotope variability among mantle melts. *Contributions to*
855 *mineralogy and petrology*, 133(1), 1-11. <https://doi.org/10.1007/s004100050432>

856 Verdel, C., Campbell, M. J., & Allen, C. M., 2021. Detrital zircon petrochronology of
857 central Australia, and implications for the secular record of zircon trace element
858 composition. *Geosphere*, 17(2), 538-560. <https://doi.org/10.1130/GES02300.1>

859 Wang Q. F., Deng J., Li, C.S., Li, G. J., Li, Y., Qiao, L., 2014. The boundary between
860 the Simao and Yangtze blocks and their locations in Gondwana and Rodinia:
861 Constraints from detrital and inherited zircons. *Gondwana Research*, 26(2):438-448.
862 <https://doi.org/10.1016/j.gr.2013.10.002>

863 Wang, J. Q., Shu, L. S., & Santosh, M., 2017b. U-Pb and Lu-Hf isotopes of detrital
864 zircon grains from Neoproterozoic sedimentary rocks in the central Jiangnan
865 Orogen, South China: Implications for Precambrian crustal evolution. *Precambrian*
866 *Research*, 294, 175-188. <https://doi.org/10.1016/j.precamres.2017.03.025>

867 Wang, J. Q., Shu, L. S., Santosh, M. & Xu, Z. Q., 2015. The pre-Mesozoic crustal
868 evolution of the Cathaysia Block, South China: insights from geological
869 investigation, zircon U-Pb geochronology, Hf isotope and REE geochemistry from
870 the Wugongshan complex. *Gondwana Research*, 28(1), 225-245. DOI:
871 10.1016/j.gr.2014.03.008

872 Wang, J., & Li, Z. X., 2003. History of Neoproterozoic rift basins in South China:

873 implications for Rodinia break-up. *Precambrian Research*, 122(1-4), 141-158.
874 [https://doi.org/10.1016/S0301-9268\(02\)00209-7](https://doi.org/10.1016/S0301-9268(02)00209-7)

875 Wang, K. X., Sun, L. Q., Sun, T., Huang, H., & Qin, L. S., 2018c. Provenance,
876 weathering conditions, and tectonic evolution history of the Cambrian
877 meta-sediments in the Zhuguangshan area, Cathaysia Block. *Precambrian Research*,
878 311, 195-210. <https://doi.org/10.1016/j.precamres.2018.04.011>

879 Wang, L. J., Yu, J. H., Griffin, W. L. & O'Reilly, S.Y., 2012a. Early crustal evolution
880 in the western Yangtze block: evidence from U-Pb and Lu-Hf isotopes on detrital
881 zircons from sedimentary rocks. *Precambrian Research*, 222-223, 368-385.
882 <https://doi.org/10.1016/j.precamres.2011.08.001>

883 Wang, P. M., Yu, J. H., Sun, T., Ling, H. F., Chen, P. R., Zhao, K. D., Chen, W. F. &
884 Liu, Q., 2012b. Geochemistry and detrital zircon geochronology of Neoproterozoic
885 sedimentary rocks in eastern Hunan Province and their tectonic significance. *Acta*
886 *Petrologica Sinica*, 28(12), 3841-3857. (in Chinese with English abstract)

887 Wang, P. M., Yu, J. H., Sun, T., Shi, Y., Chen, P. R., Zhao, K. D., Chen, W. F., & Liu,
888 Q., 2013a. Composition variations of the Sinian-Cambrian sedimentary rocks in
889 Hunan and Guangxi provinces and their tectonic significance. *Science China-Earth*
890 *Sciences*, 56(11), 1899-1917. DOI: 10.1007/s11430-013-4634-1

891 Wang, W., Cawood, P. A., Pandit, M. K., Xia, X. P., Raveggi, M., Zhao, J. H., Zheng,
892 J. P., & Qi, L., 2021. Fragmentation of South China from greater India during the
893 Rodinia-Gondwana transition. *Geology*, 49(2), 228-232. DOI: 10.1130/G48308.1

894 Wang, W., Cawood, P. A., Pandit, M. K., Zhao, J. H., & Zheng, J. P., 2019a. No
895 collision between Eastern and Western Gondwana at their northern extent. *Geology*,
896 47(4), 308-798. <https://doi.org/10.1130/G45745.1>

897 Wang, W., Cawood, P. A., Zhou, M. F., Pandit, M. K., Xia, X. P., & Zhao, J. H., 2017a.
898 Low-delta O-18 Rhyolites from the Malani Igneous Suite: A Positive Test for South
899 China and NW India Linkage in Rodinia. *Geophysical Research Letters*, 44(20),
900 10298-10305. DOI: 10.1002/2017GL074717

901 Wang, W., Zeng, M. F., Zhou, M. F., Zhao, J. H., Zheng, J. P., & Lan, Z. F., 2018b.
902 Age, provenance and tectonic setting of Neoproterozoic to early Paleozoic

903 sequences in southeastern South China block: constraints on its linkage to western
904 Australia-east Antarctica. *Precambrian Research*, 309, 290-308.
905 <https://doi.org/10.1016/j.precamres.2017.03.002>

906 Wang, X. C., Li, X. H., Li, W. X., & Li, Z. X., 2007a. Ca. 825 Ma komatiitic basalts
907 in South China: First evidence for > 1500 °C mantle melts by a Rodinian mantle
908 plume. *Geology*, 35(12), 1103-1106. <https://doi.org/10.1130/G23878A.1>

909 Wang, X. C., Li, X. H., Li, Z. X., Li, Q. L., Tang, G. Q., Gao, Y. Y., Zhang, Q. R., &
910 Liu, Y., 2012c. Episodic Precambrian crust growth: Evidence from U-Pb ages and
911 Hf-O isotopes of zircon in the Nanhua Basin, central South China. *Precambrian*
912 *Research*, 222, 386-403. DOI: 10.1016/j.precamres.2011.06.001

913 Wang, X. C., Li, Z. X., Li, X. H., Li, Q. L., Tang, G. Q., Zhang, Q. R., Liu, Y., 2011.
914 Nonglacial origin for low-delta O-18 Neoproterozoic magmas in the South China
915 Block: Evidence from new in-situ oxygen isotope analyses using SIMS. *Geology*,
916 39(8), 735-738. DOI: 10.1130/G31991.1

917 Wang, X. L., Zhou, J. C., Griffin, W. L., Wang, R. C., Qiu, J. S., Reilly, S. Y. O., Xu,
918 X. S., Liu, X. M. & Zhang, G. L., 2007b. Detrital zircon geochronology of
919 Precambrian basement sequences in the Jiangnan Orogen: dating the assembly of
920 the Yangtze and Cathaysia Blocks. *Precambrian Research*, 159(1-2), 117-131.
921 <https://doi.org/10.1016/j.precamres.2007.06.005>

922 Wang, X. L., Zhou, J. C., Wan, Y. S., Kitajima, K., Wang, D., Bonamici, C., Qiu, J. S.
923 & Sun, T., 2013b. Magmatic evolution and crustal recycling for Neoproterozoic
924 strongly peraluminous granitoids from southern China: Hf and O isotopes in zircon.
925 *Earth and Planetary Science Letters*, 366, 71-82.
926 <https://doi.org/10.1016/j.epsl.2013.02.011>

927 Wang, Y. J., Zhang, F. F., Fan, W. M., Zhang, G. W., Chen, S. Y., Cawood, P. A.,
928 Zhang, A. M., 2010. Tectonic setting of the South China Block in the early
929 Paleozoic: Resolving intracontinental and ocean closure models from detrital zircon
930 U-Pb geochronology. *Tectonics*, 29(6), 1-16. DOI: 10.1029/2010TC002750

931 Wang, Z. H., Yang, W. Q., Zhou, D., Niu, Z. J., He, Y. Y., Song, F., 2018a. Detrital
932 Zircon U-Pb Geochronological Records and Its Response of Provenance

933 Transformation of Strata Surrounding Cambrian-Devonian Unconformity in
934 Eastern Margin of Yunkai Massif. *Earth Science*, 43(11): 4193-4203. (in Chinese
935 with English abstract). [https:// doi.org/10.3799/dqkx.2018.242](https://doi.org/10.3799/dqkx.2018.242)

936 Wu, L., Jia, D., Li, H. B., Deng, F. & Li, Y. Q., 2010. Provenance of detrital zircons
937 from the Late Neoproterozoic to Ordovician sandstones of South China:
938 implications for its continental affinity. *Geological Magazine*, 147(06), 974-980.
939 DOI: 10.1017/S0016756810000725

940 Wu, P., Zhang, S. B., Zheng, Y. F., Li, Q. L., Li, Z. X., & Sun, F. Y., 2020. The
941 occurrence of Neoproterozoic low delta O-18 igneous rocks in the northwestern
942 margin of the South China Block: Implications for the Rodinia configuration.
943 *Precambrian Research*, 347, 105841. DOI: 10.1016/j.precamres.2020.105841

944 Wu, Y. W., 2013. The evolution record of Longmuco-Shuanghu-Lancang
945 Ocean-Cambrian-Permian ophiolites. (Doctoral dissertation). Changchun, Jilin:
946 Jilin University. (in Chinese with English abstract).

947 Xiang, L. and Shu, L. S., 2010. Pre-Devonian tectonic evolution of the eastern South
948 China Block: Geochronological evidence from detrital zircons. *Science China
949 Earth Science*, 40(10): 1377-1388. (in Chinese with English abstract) DOI:
950 10.1007/s11430-010-4061-5

951 Xiong, C., Niu, Y. L., Chen, H. D., Chen, A. Q., Zhang, C. G., Li, F., Yang, S. & Xu, S.
952 L., 2019. Detrital zircon U-Pb geochronology and geochemistry of late
953 Neoproterozoic-early Cambrian sedimentary rocks in the Cathaysia block:
954 constraint on its palaeo-position in Gondwana supercontinent. *Geological
955 Magazine*, 156(9), 1587-1604. DOI: <https://doi.org/10.1017/S0016756819000013>

956 Xu, Y. J., Cawood, P. A., Du, Y. S., Hu, L. S., Yu, W. C., Zhu, Y. H., & Li, W. C., 2013.
957 Linking South China to northern Australia and India on the margin of Gondwana:
958 Constraints from detrital zircon U-Pb and Hf isotopes in Cambrian strata. *Tectonics*,
959 32(6), 1547-1558. <https://doi.org/10.1002/tect.20099>

960 Xu, Y. J., Cawood, P. A., Du, Y. S., Huang, H. W., & Wang, X. Y., 2014. Early
961 Paleozoic orogenesis along Gondwana's northern margin constrained by
962 provenance data from South China. *Tectonophysics*, 636, 40-51.

963 <https://doi.org/10.1016/j.tecto.2014.08.022>

964 Xue, E. K., Wang, W., Huang, S. F., & Lu, G. M., 2019. Detrital zircon U-Pb-Hf
965 isotopes and whole-rock geochemistry of Neoproterozoic-Cambrian successions in
966 the Cathaysia Block of South China: Implications on paleogeographic
967 reconstruction in supercontinent. *Precambrian Research*, 331, 105348.
968 <https://doi.org/10.1016/j.precamres.2019.105348>

969 Yan, C. L., Shu, L. S., Faure, M., Chen, Y., & Huang, R. B., 2019. Time constraints on
970 the closure of the Paleo-South China Ocean and the Neoproterozoic assembly of
971 the Yangtze and Cathaysia blocks: Insight from new detrital zircon analyses.
972 *Gondwana Research*, 73, 175-189. <https://doi.org/10.1016/j.gr.2019.03.018>

973 Yan, C. L., Shu, L. S., Santosh, M., Yao, J. L., Li, J. Y., & Li, C., 2015. The
974 Precambrian tectonic evolution of the western Jiangnan Orogen and western
975 Cathaysia Block: Evidence from detrital zircon age spectra and geochemistry of
976 clastic rocks. *Precambrian Research*, 268, 33-60.
977 <https://doi.org/10.1016/j.precamres.2015.07.002>

978 Yang, C., Li, X. H., Wang, X. C., & Lan, Z., 2015. Mid-Neoproterozoic angular
979 unconformity in the Yangtze Block revisited: insights from detrital zircon U-Pb age
980 and Hf-O isotopes. *Precambrian Research*, 266, 165-178.
981 <https://doi.org/10.1016/j.precamres.2015.05.016>

982 Yang, Y. N., Wang, X. C., Li, Q. L., & Li, X. H., 2016. Integrated in situ U-Pb age and
983 Hf-O analyses of zircon from Suixian Group in northern Yangtze: New insights into
984 the Neoproterozoic low-delta O-18 magmas in the South China Block.
985 *Precambrian Research*, 273, 151-164. DOI: 10.1016/j.precamres.2015.12.008

986 Yang, Z. Y., & Jiang, S. Y., 2019. Detrital zircons in metasedimentary rocks of
987 Mayuan and mamianshan group from Cathaysia block in northwestern Fujian
988 province, South China: new constraints on their formation ages and
989 paleogeographic implication. *Precambrian Research*, 320, 13-30.
990 <https://doi.org/10.1016/j.precamres.2018.10.004>

991 Yang, Z. Y., Sun, Z. M., Yang, T. S., & Pei, J. L., 2004. A Long Connection (750-380
992 Ma) between South China and Australia: Paleomagnetic Constraints. *Earth and*

993 *Planetary Science Letters*, 220, 423-434.
994 [https://doi.org/10.1016/S0012-821X\(04\)00053-6](https://doi.org/10.1016/S0012-821X(04)00053-6)

995 Yao, J. L., Cawood, P. A., Shu, L. S., & Zhao, G. C., 2019. Jiangnan Orogen, South
996 China: A similar to 970-820 Ma Rodinia margin accretionary belt. *Earth Science*
997 *Reviews*, 196, 102872. DOI: 10.1016/j.earscirev.2019.05.016

998 Yao, J. L., Shu, L. S. & Santosh, M., 2011. Detrital zircon U-Pb geochronology,
999 Hf-isotopes and geochemistry-new clues for the Precambrian crustal evolution of
1000 Cathaysia block, South China. *Gondwana Research*, 20(2-3), 553-567.
1001 <https://doi.org/10.1016/j.gr.2011.01.005>

1002 Yao, W. H., Li, Z. X., Li, W. X., Li, X. H., & Yang, J. H., 2014. From Rodinia to
1003 Gondwanaland: a tale of detrital zircon provenance analyses from the southern
1004 Nanhua basin, South China. *American Journal of Science*, 314(1), 278-313.
1005 DOI:10.2475/01.2014.08

1006 Yao, W. H., Li, Z. X., Li, W. X., Su, L. & Yang, J. H., 2015. Detrital provenance
1007 evolution of the Ediacaran-Silurian Nanhua Foreland basin, South China.
1008 *Gondwana Research*, 2015, 28(4), 1449-1488. DOI: 10.1016/j.gr.2014.10.018

1009 Yu, J. H., Reilly, S. Y. O, Wang, L. J., Griffin, W. L., Zhou, M. F., Zhang, M. & Shu, L.
1010 S., 2010. Components and episodic growth of Precambrian crust in the Cathaysia
1011 block, South China: evidence from U-Pb ages and Hf isotopes of zircons in
1012 Neoproterozoic sediments. *Precambrian Research*, 181(1-4), 97-114.
1013 <https://doi.org/10.1016/j.precamres.2010.05.016>

1014 Yuan, H. Y., Zhou, Q., Ding, J., Zhang, H. H., Zhu, L. T., Liang, J., Tang, G. L., &
1015 Wang, C. N., 2017. U-Pb Geochronological Studies on Detrital Zircon in Jianglang
1016 Group, Western Sichuan Province, China. *Acta Mineralogical Sinica*, 37(3),
1017 296-304. DOI: 10.1016/j.lithos.2021.106108 (in Chinese with English abstract)

1018 Yuan, X. Y., Niu, M. L., Cai, Q. R., Wu, Q., Zhu, G., Li, X. C., Sun, Y., & Li, C., 2021.
1019 Bimodal volcanic rocks in the northeastern margin of the Yangtze Block: Response
1020 to breakup of Rodinia supercontinent. *Lithos*, 390, 106108. DOI:
1021 10.1016/j.lithos.2021.106108

1022 Zhang, H., Liu, Y. X., Ding, X. Z., Gao, L. Z., Yang, C., Zhang, J. B., Gong, C. Q. &

1023 Liu, H. G., 2020a. Geochronology, Geochemistry, Whole Rock Sr-Nd and Zircon
1024 Hf-O Isotopes of the Early Neoproterozoic Volcanic Rocks in Jiangshan, Eastern
1025 Part of the Jiangnan Orogen: Constraints on Petrogenesis and Tectonic Implications.
1026 *Acta Geologica Sinica-English Edition*, 94(4), 1117-1137. DOI:
1027 10.1111/1755-6724.14561

1028 Zhang, J. B., Ni, J. B., Liu, Y. X., Zhang, H., & Bu, L., 2020b. Ordovician Proto-basin
1029 in South China and its Tectonic Implications: Evidence from the Detrital Zircon
1030 U-Pb Ages of the Ordovician in Central Hunan, China. *Acta Geologica
1031 Sinica-English Edition*, 94(6), 2115-2133. DOI:10.1111/1755-6724.14583

1032 Zhang, J. W., Ye, T. P., Dai, Y. R., Chen, J. S., Zhang, H., Dai, C. G., Yuan, G. H. &
1033 Jiang, K. Y., 2019a. Provenance and tectonic setting transition as recorded in the
1034 Neoproterozoic strata, western Jiangnan Orogen: Implications for South China
1035 within Rodinia. *Geoscience Frontiers*, 10(5), 1823-1839.
1036 <https://doi.org/10.1016/j.gsf.2018.10.009>

1037 Zhang, X. C., Wang, Y. J., Clift, P. D. Yan, Y., Zhang, Y. Z. & Zhang, L., 2018.
1038 Paleozoic Tectonic Setting and Paleogeographic Evolution of the Qin-Fang Region,
1039 Southern South China Block: Detrital Zircon U-Pb Geochronological and Hf
1040 Isotopic Constraints. *Geochemistry, Geophysics, Geosystems*, 19(10), 3962-3979.
1041 <https://doi.org/10.1029/2018GC007713>

1042 Zhang, X. Z., Dong, Y. S., Li, C., Deng, M. R., Zhang, L. & Xu, W., 2014. Silurian
1043 high-pressure granulites from Central Qiangtang, Tibet: constraints on early
1044 Paleozoic collision along the northeastern margin of Gondwana. *Earth and
1045 Planetary Science Letters*, 405, 39-51. DOI: 10.1016/j.epsl.2014.08.013

1046 Zhang, Y. L., Jia, X. T., Wang, Z. Q., Wang, K. M., Chen, M. Y., 2019b.
1047 Paleogeography and provenance analysis of Early Cambrian Xiannvdong
1048 Formation in the Micangshan area. *Acta Geologica Sinica*, 93(11): 2904-2920.
1049 DOI:10.19762/j.cnki.dizhixuebao.2019094. (in Chinese with English abstract)

1050 Zhao, B. X., Long, X. P., Luo, J., Dong, Y. P., Lan, C. Y., Wang, J. Y. & Wu, B., 2021.
1051 Late Neoproterozoic to early Paleozoic paleogeographic position of the Yangtze
1052 block and the change of tectonic setting in its northwestern margin: Evidence from

1053 detrital zircon U-Pb ages and Hf isotopes of sedimentary rocks. *GSA Bulletin*.
1054 <https://doi.org/10.1130/B35980.1>

1055 Zhao, G. C. & Cawood, P. A., 1999. Tectonothermal evolution of the Mayuan
1056 Assemblage in the Cathaysia Block; implications for Neoproterozoic
1057 collision-related assembly of the South China Craton. *American Journal of Science*,
1058 299 (4), 309-339. DOI: <https://doi.org/10.2475/ajs.299.4.309>

1059 Zhao, G. C., Wang, Y. J., Huang, B. C., Dong, Y. P., Li, S. Z., Zhang, G. W. & Yu, S.,
1060 2018a. Geological reconstructions of the East Asian blocks: from the breakup of
1061 Rodinia to the assembly of Pangea. *Earth Science Reviews*, 186, 262-286. DOI:
1062 10.1016/j.earscirev.2018.10.003

1063 Zhao, J. H., Asimow, P. D., Zhou, M. F., Zhang, J., Yan, D. P., & Zheng, J. P., 2017.
1064 An Andean-type arc system in Rodinia constrained by the Neoproterozoic Shimian
1065 ophiolite in South China. *Precambrian Research*, 296, 93-111.
1066 <https://doi.org/10.1016/j.precamres.2017.04.017>

1067 Zhao, J. H., Pandit, M. K., Wang, W., & Xia, X. P., 2018b. Neoproterozoic
1068 tectonothermal evolution of NW India: Evidence from geochemistry and
1069 geochronology of granitoids. *Lithos*, 316, 330-346.
1070 DOI:10.1016/j.lithos.2018.07.020

1071 Zhao, J. H., Pandit, M. K., Wang, W., & Xia, X. P., 2018c. Neoproterozoic
1072 tectonothermal evolution of NW India: Evidence from geochemistry and
1073 geochronology of granitoids. *Lithos*, 316, 330-346.
1074 DOI:10.1016/j.lithos.2018.07.020

1075 Zhao, J. H., Zhou, M. F., Yan, D. P., Yang, Y. H., & Sun, M., 2008. Zircon Lu-Hf
1076 isotopic constraints on Neoproterozoic subduction-related crustal growth along the
1077 western margin of the Yangtze Block, South China. *Precambrian Research*,
1078 163(3-4), 189-209. <https://doi.org/10.1016/j.precamres.2007.11.003>

1079 Zhao, J. H., Zhou, M. F., Yan, D. P., Zheng, J. P., & Li, J. W., 2011. Reappraisal of the
1080 ages of Neoproterozoic strata in South China: no connection with the Grenvillian
1081 orogeny. *Geology*, 39(4), 299-302. <https://doi.org/10.1130/G31701.1>

1082 Zhao, J. H., Zhou, M. F., Zheng, J. P., & Fang, S. M., 2010. Neoproterozoic crustal

1083 growth and reworking of the Northwestern Yangtze Block: constraints from the
1084 Xixiang dioritic intrusion, South China. *Lithos*, 120(3-4), 439-452.
1085 <https://doi.org/10.1016/j.lithos.2010.09.005>

1086 Zhao, Z. B., Xu, Z. Q., Ma, X. X., Liang, F. H., & Guo, P., 2018d.
1087 Neoproterozoic-Early Paleozoic tectonic evolution of the South China Craton: New
1088 insights from the polyphase deformation in the southwestern Jiangnan orogen. *Acta*
1089 *Geologica Sinica-English Edition*, 92(5), 1700-1727.
1090 <https://doi.org/10.1111/1755-6724.13672>

1091 Zhou, J. L., 2015b. Tectonic affinity of the Neoproterozoic-aged Imorona-Itsindro
1092 Suite in Masagascar and its geological significance. China University of
1093 Geosciences (Beijing). (in Chinese with English abstract).

1094 Zhou, J. L., Li, X. H., & Tucker, R. D., 2020. New insights into the genesis of
1095 Neoproterozoic low-delta O-18 granitoids in the Seychelles: crustal cannibalization
1096 within an intra-plate extensional setting. *Science Bulletin*, 65(22), 1880-1883. DOI:
1097 [10.1016/j.scib.2020.07.025](https://doi.org/10.1016/j.scib.2020.07.025)

1098 Zhou, J. L., Li, X. H., Tang, G. Q., Liu, Y., & Tucker, R. D., 2017. New evidence for a
1099 continental rift tectonic setting of the Neoproterozoic Imorona-Itsindro Suite
1100 (central Madagascar). *Precambrian Research*, 306, 94-111. DOI:
1101 [10.1016/j.precamres.2017.12.029](https://doi.org/10.1016/j.precamres.2017.12.029)

1102 Zhou, J. L., Li, X. H., Tang, G. Q., Liu, Y., & Tucker, R. D., 2018a. New evidence for
1103 a continental rift tectonic setting of the Neoproterozoic Imorona-Itsindro Suite
1104 (central Madagascar). *Precambrian Research*, 306, 94-111. DOI:
1105 [10.1016/j.precamres.2017.12.029](https://doi.org/10.1016/j.precamres.2017.12.029)

1106 Zhou, J. L., Shao, S., Luo, Z. H., Shao, J. B., Wu, D. T., & Rasoamalala, V., 2015a.
1107 Geochronology and geochemistry of Cryogenian gabbros from the
1108 Ambatondrazaka area, east-central Madagascar: Implications for Madagascar-India
1109 correlation and Rodinia paleogeography. *Precambrian Research*, 256,
1110 256-270. <https://doi.org/10.1016/j.precamres.2014.11.005>

1111 Zhou, M. F., Ma, Y., Yan, D. P., Xia, X., Zhao, J. H., & Sun, M., 2006. The Yanbian
1112 terrane (Southern Sichuan Province, SW China): a Neoproterozoic arc assemblage

1113 in the western margin of the Yangtze block. *Precambrian Research*, 144(1-2),
1114 19-38. <https://doi.org/10.1016/j.precamres.2005.11.002>

1115 Zhou, X. Y., Yu, J. H., O'Reilly, S. Y., Griffin, W. L., Sun, T., Wang, X. L., Tran, M. D.
1116 & Nguyen, D. L., 2018b. Component variation in the late Neoproterozoic to
1117 Cambrian sedimentary rocks of SW China-NE Vietnam, and its tectonic
1118 significance. *Precambrian Research*, 308, 92-110.
1119 DOI:10.1016/j.precamres.2018.02.003

1120 Zhu, D. C., Zhao, Z. D., Niu, Y. L., Dilek, Y., Wang, L. Q., & Mo, X. X., 2011. Lhasa
1121 terrane in Southern Tibet came from Australia. *Geology*, 39(8), 727-730. DOI:
1122 10.1130/G31895.1

1123 Zhu, G. L., Yu, J. H., Zhou, X. Y., Wang, X. L., & Wang, Y. D., 2019d. The western
1124 boundary between the Yangtze and Cathaysia blocks, new constraints from the
1125 Pingbian Group sediments, southwest South China Block. *Precambrian Research*,
1126 331, 105350. <https://doi.org/10.1016/j.precamres.2019.105350>

1127 Zhu, Y., Lai, S. C., Qin, J. F., Zhu, R. Z., Zhang, F. Y., Zhang, Z. Z., & Zhao, S. W.,
1128 2019a. Neoproterozoic peraluminous granites in the western margin of the Yangtze
1129 Block, South China: Implications for the reworking of mature continental crust.
1130 *Precambrian Research*, 333, 105443. DOI: 10.1016/j.precamres.2019.105443

1131 Zou, H., Bagas, L., Li, X. Y., Liu, H., Jiang, X. W. & Li, Y., 2020. Origin and
1132 evolution of the Neoproterozoic Dengganping Granitic Complex in the western
1133 margin of the Yangtze Block, SW China: Implications for breakup of Rodina
1134 Supercontinent. *Lithos*, 370-371, 1-21. DOI: 10.1016/j.lithos.2020.105602

1135

1136

1137

1138

1139 **Captions**

1140 **Table 1.** Location and stratigraphic information of samples analyzed

1141

1142 **Figure 1.** Simplified geological maps of (a) the Tibetan Plateau (after Tian et al., 2020), (b) the

1143 Yidun Terrane (after Peng et al., 2014), (c) the Gongling region of the Eastern Yidun subterrane

1144 (after BGMRS, 1980, 1984) and (d) the Cryogenian-Ordovician strata and samples in the

1145 Gongling region (after BGMRS, 1980, 1984). Abbreviations: ADFB, Aravalli-Delhi fold belt;

1146 CITZ, Central Indian tectonic zone; EGB, East Ghats belt; EYD, Eastern Yidun subterrane; WYD,

1147 Western Yidun subterrane.

1148

1149 **Figure 2.** Photographs of the representative (meta-)sedimentary samples from the Eastern Yidun

1150 subterrane. (a and b) the schist samples, (c) the sandstone sample, and (d) the slate sample.

1151 Abbreviations: Qtz, quartz; Pl, plagioclase; Mca, mica.

1152

1153 **Figure 3.** Concordia and detrital zircon age histogram-probability density distribution diagrams of

1154 the Neoproterozoic-Ordovician samples from the Eastern Yidun subterrane.

1155

1156 **Figure 4.** Plots of zircon $\epsilon_{\text{Hf}}(t)$ versus U-Pb age of the Neoproterozoic (a) and Ordovician (b)

1157 detrital sediments in the Eastern Yidun subterrane. The detrital zircons $\epsilon_{\text{Hf}}(t)$ data from the Yidun

1158 terrane (this study and Tian et al., 2020). The igneous zircons $\epsilon_{\text{Hf}}(t)$ values of the Panxi-Hannan

1159 arc (data sources: Ao et al., 2019; Li et al., 2018; Qi & Zhao, 2020; Zhao et al., 2008a, 2010, 2017;

1160 Zhao et al., 2008b; Zhu et al., 2019a); The igneous zircons $\epsilon_{\text{Hf}}(t)$ values of the Jiangnan Orogen

1161 (data sources: Yao et al., 2019, and references therein).

1162

1163 **Figure 5.** Detrital zircon age distributions for late Tonian to Ordovician rocks from Yidun, South
1164 China, India and Australia terranes. **Compilation of zircon age distribution of**
1165 Neoproterozoic-Early Paleozoic sedimentary rocks from (A1-3) the Yidun terrane (This study and
1166 Tian et al., 2020), (B1-5) western Yangtze terrane (This study and Chen et al., 2016, 2018, 2021;
1167 Han et al., 2017; Hofmann et al., 2016; Liu et al., 2019c; Liu et al., 2020b; Luo et al., 2020; Sun et
1168 al., 2008, 2009; Tian et al., 2020; Wang et al., 2012a; Wang et al., 2014; Xia et al., 2016; Yuan et
1169 al., 2017; Zhang et al., 2019b; Zhao et al., 2021), (C1-5) the Nanhua basin (Cui et al., 2015; He et
1170 al., 2020; Liu et al., 2019a; Liu et al., 2019b; Ma et al., 2019; Sun et al., 2018; Qi et al., 2018;
1171 Wang et al., 2012b, 2013a; Wang et al., 2007b; Wang et al., 2017b; Wang et al., 2018a; Yan et al.,
1172 2019; Yang et al., 2015; Zhang et al., 2019a; Zhang et al., 2020b; Zhao et al., 2018c; Zhou et al.,
1173 2018b; Zhu et al., 2019b), (D1-5) the Cathaysia terrane (Qi et al., 2018, 2020; Wang et al., 2010;
1174 Wang et al., 2012b; Wang et al., 2015; Wang et al., 2018a; Wang et al., 2018b; Wang et al., 2018c;
1175 Wu et al., 2010; Xiang & Shu, 2010; Xiong et al., 2019; Xu et al., 2013, 2014; Xue et al., 2019;
1176 Yan et al., 2015; Yang & Jiang, 2019; Yao et al., 2011; Yao et al., 2014, 2015; Yu et al., 2010;
1177 Zhang et al., 2018; Zhou et al., 2018b), (E1-3) the western India terrane (Hughes et al., 2019; Lan
1178 et al., 2020; Malone et al., 2008; McKenzie et al., 2013; Myrow et al., 2010; Qasim et al., 2018;
1179 Turner et al., 2014; Wang et al., 2019a), (F1-5) the Aravalli-Delhi basin (DeCelles et al., 2000;
1180 Gehrels et al., 2006; Hofmann et al., 2011; Malone et al., 2008; Mukherjee et al., 2019; Myrow et
1181 al., 2010), (G1-5) the eastern India terrane (DeCelles et al., 2000; Gehrels et al., 2006, 2011;
1182 Hughes et al., 2011; Lan et al., 2020; Long et al., 2010; Malone et al., 2008; Mckenzie et al., 2011;

1183 [McQuarrie et al., 2013](#); [Myrow et al., 2010](#); [Turner et al., 2014](#)), (H1-5) the Australia terrane
1184 ([Haines et al., 2016](#); [Johnson et al., 2016](#); [Keemana et al., 2020](#); [Mulder et al., 2020](#); [Verdel et al.,](#)
1185 [2021](#)).

1186

1187 **Figure 6.** Proposed tectonic framework and palaeogeographic position for South China, India,
1188 Seychelles and Madagascar in Rodinia during the Neoproterozoic (after [Cawood et al., 2018](#); ;
1189 [Wang et al., 2017a, 2021](#); [Zhao et al., 2018b](#)). Abbreviation: YD, Yidun Terrane. The
1190 Neoproterozoic igneous zircons $\varepsilon_{\text{Hf}}(t)$ and $\delta^{18}\text{O}$ data of the Madagascar terrane from ([Armistead et](#)
1191 [al., 2019](#); [Zhou et al., 2015, 2017](#)); of the Seychelles terrane from ([Harris & Ashwal, 2002](#);
1192 [Shellnutt et al., 2020](#); [Zhou et al., 2020](#)); of the NW India from ([Wang et al., 2017a](#)); of the
1193 western Yangzte terrane from ([Jiang et al., 2020](#); [Qi & Zhao, 2020](#); [Wu et al., 2020](#); [Yang et al.,](#)
1194 [2016](#); [Zou et al., 2020](#)); of the Aravalli-Nanhua rift basin from ([Huang et al., 2018](#); [Wang et al.,](#)
1195 [2011, 2012c](#); [Yuan et al., 2021](#); [Zhao et al., 2018b](#)).

1196

1197 **Figure 7.** Depositional setting of the Cryogenian Qiasi Group in the Eastern Yidun subterrane as
1198 inferred by discrimination plot of cumulative proportions vs. CA-DA of analyzed detrital zircons
1199 (after [Cawood et al., 2012](#)). Data are compiled from [this study](#) and [Tian et al. \(2020\)](#).

1200

1201 **Figure 8.** Tentative tectonic reconstruction models of South China (including the Yidun Terrane)
1202 along with other ambient terranes in Gondwana during Late Ediacaran-Early Cambrian (A) and
1203 Middle Cambrian-Early Ordovician (B) times (after [Zhao et al., 2018a](#)). Abbreviations: SC, South
1204 China; NC, North China.

Figure 1.

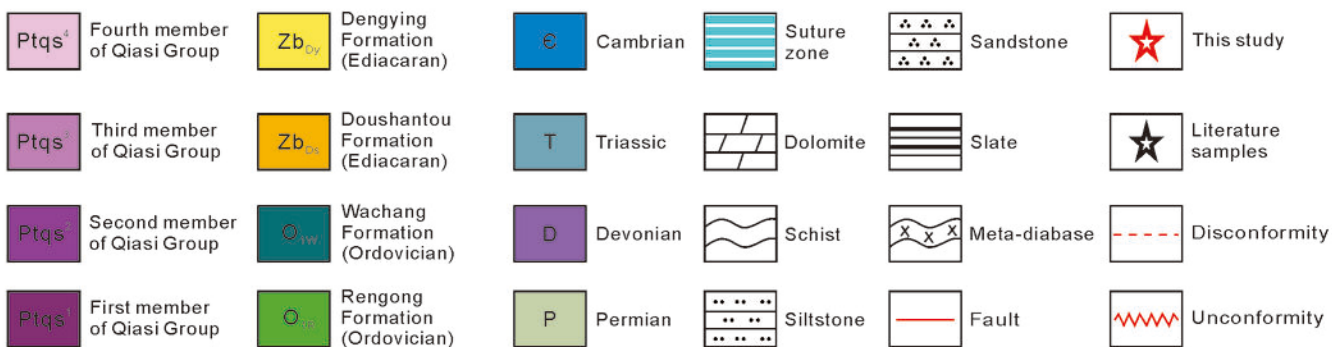
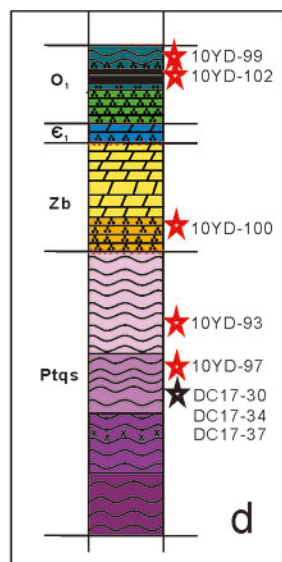
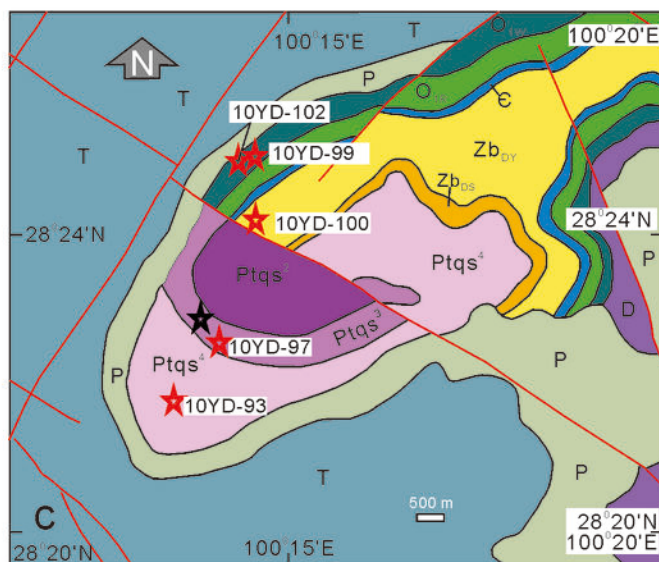
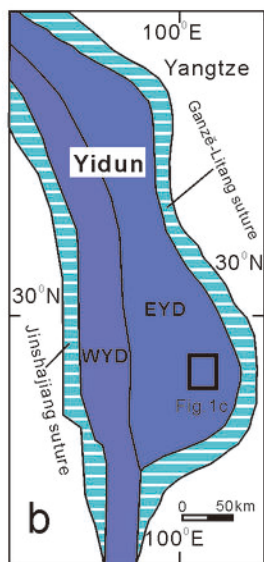
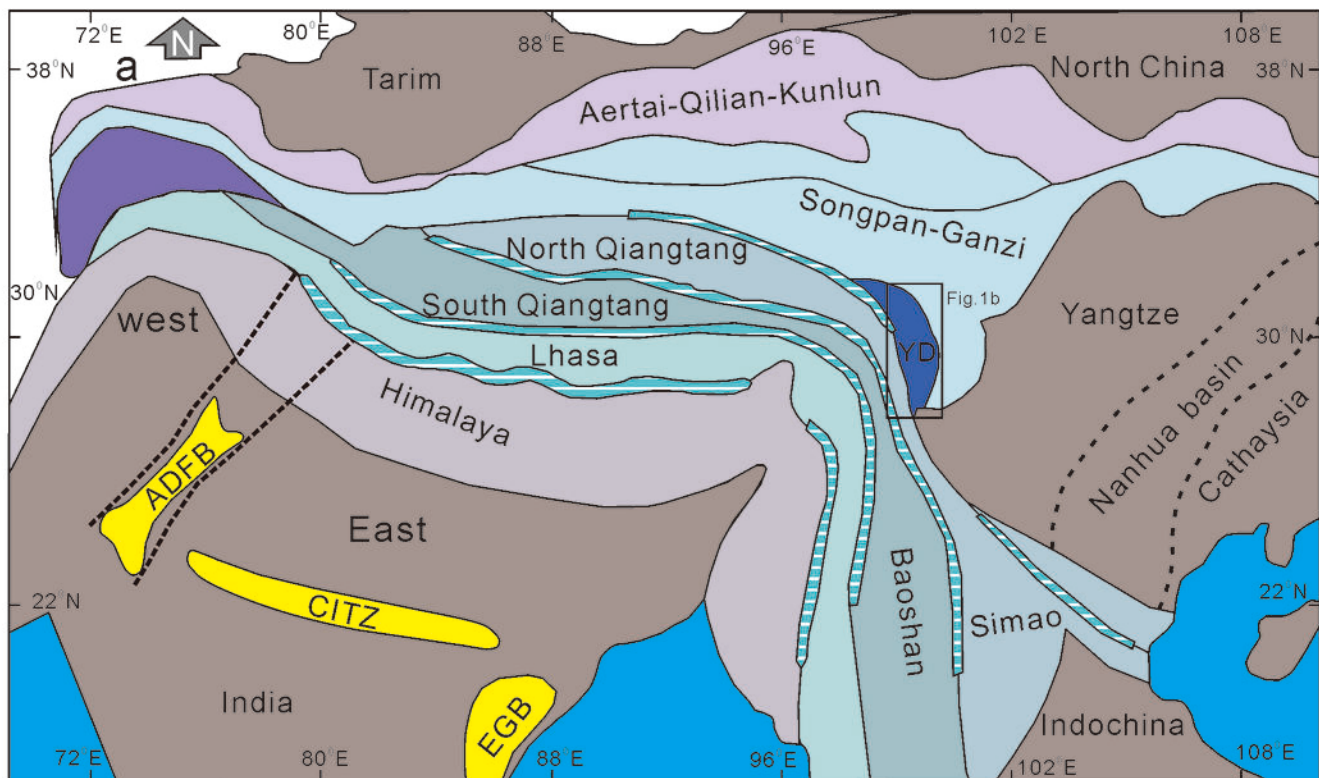


Figure 2.

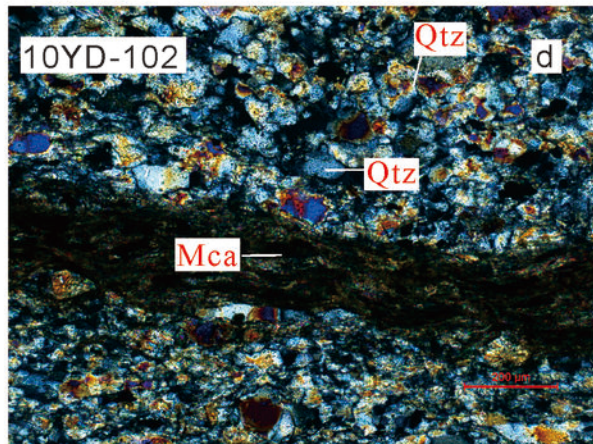
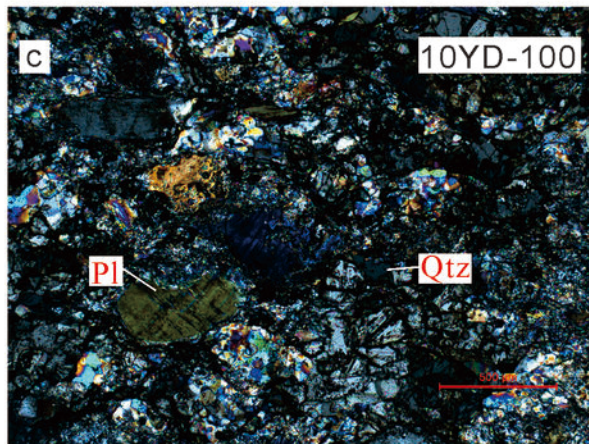
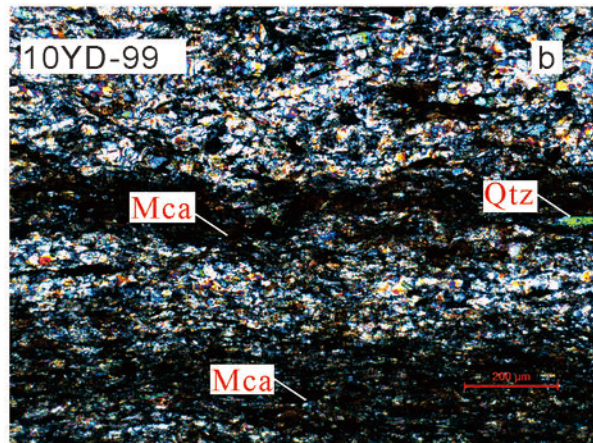
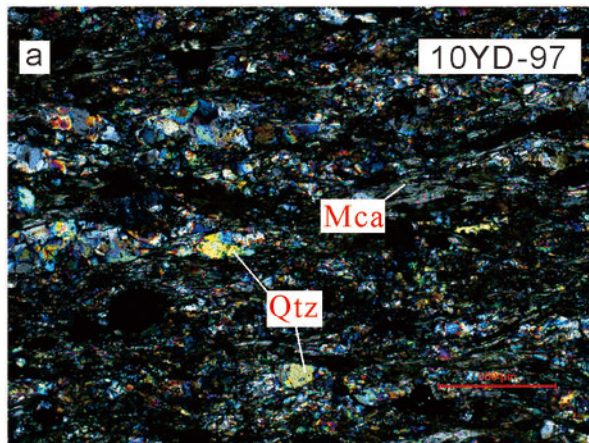


Figure 3.

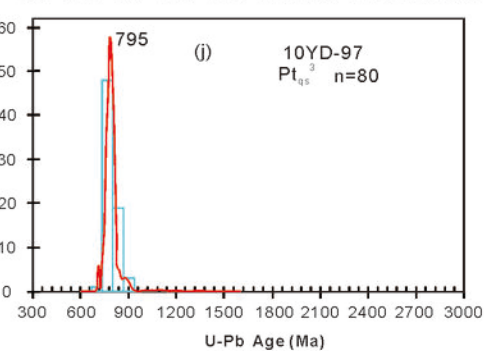
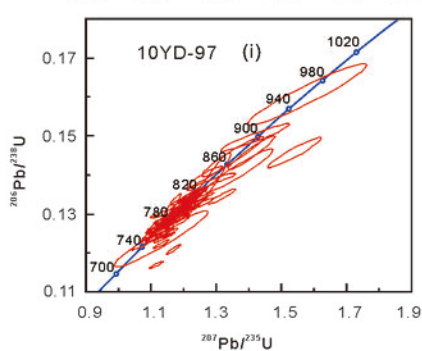
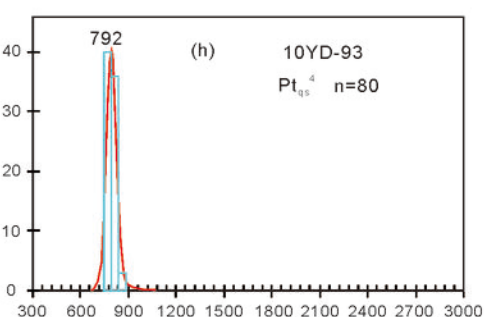
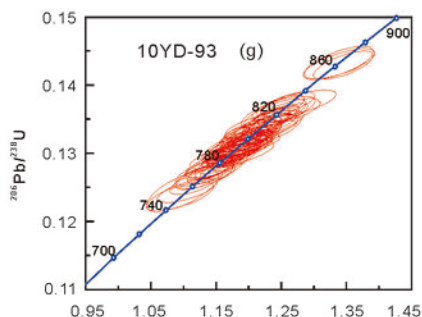
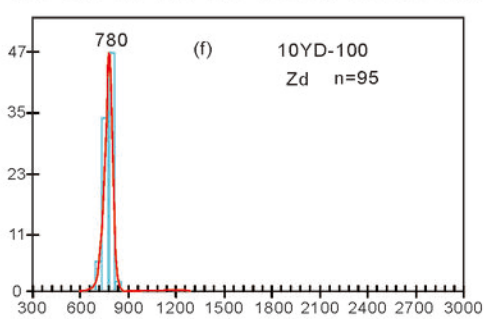
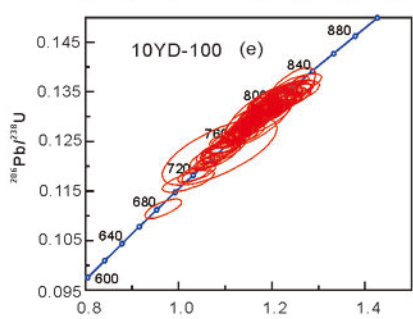
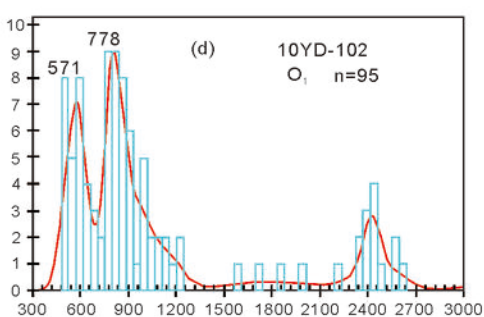
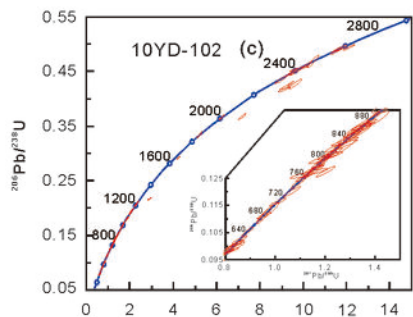
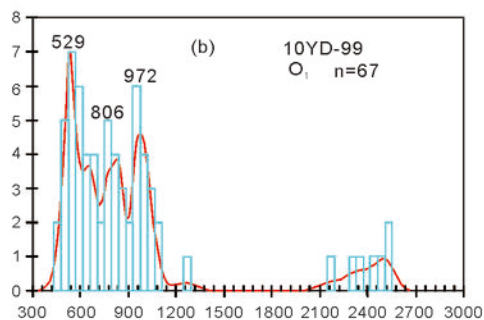
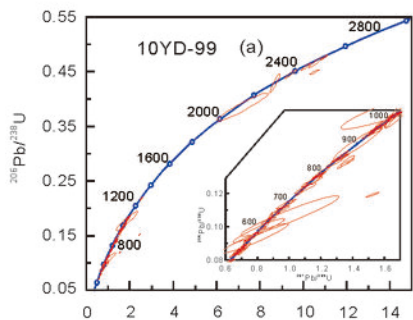


Figure 4.

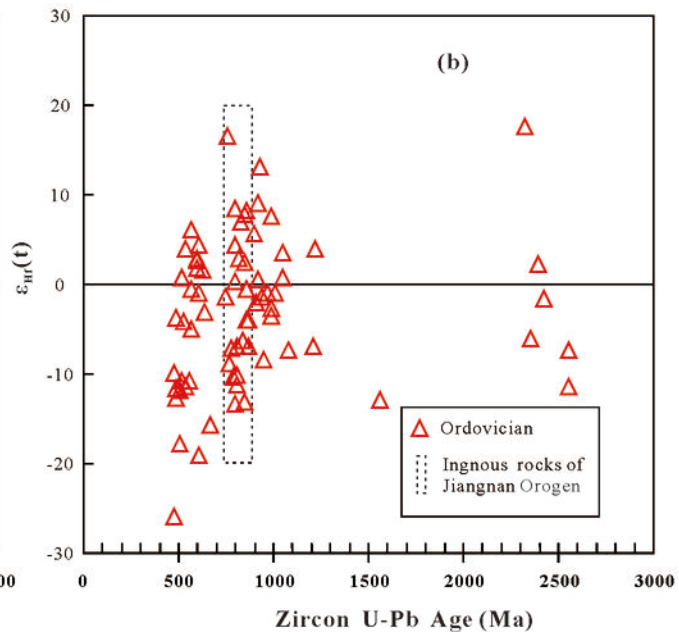
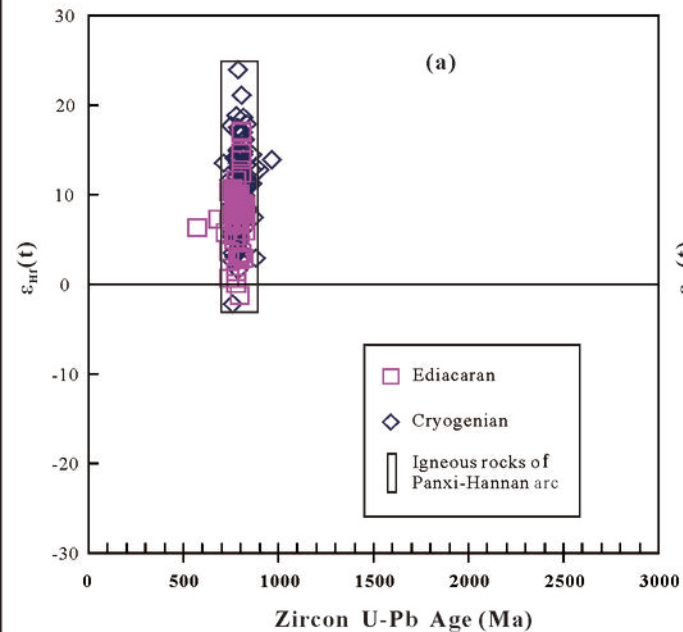


Figure 5.

Yidun

South China

India (including Himalaya)

Australia

West Yangtze

Nanhua basin

Cathaysia

Western

Aravalli-Delhi basin

Eastern

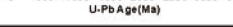
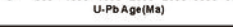
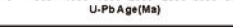
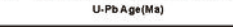
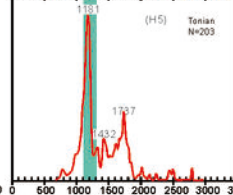
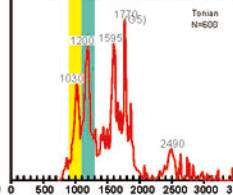
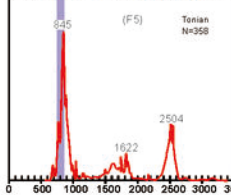
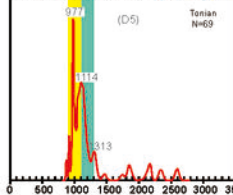
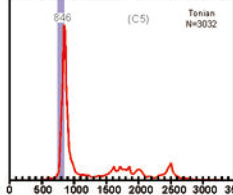
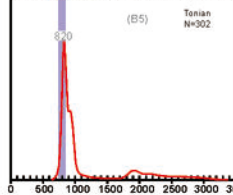
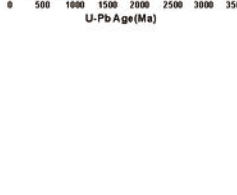
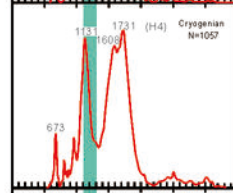
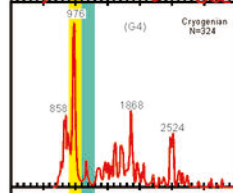
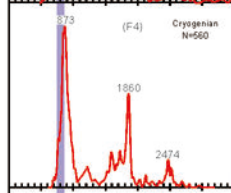
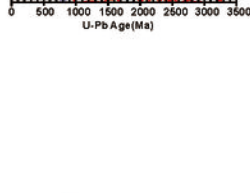
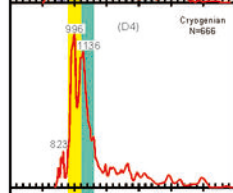
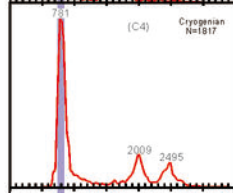
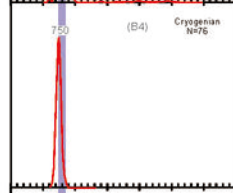
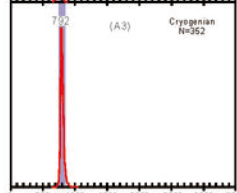
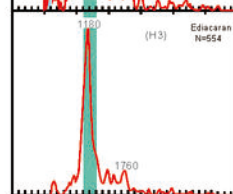
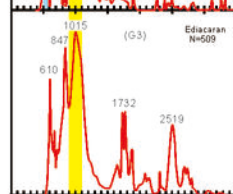
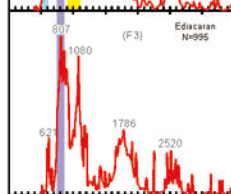
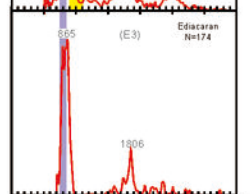
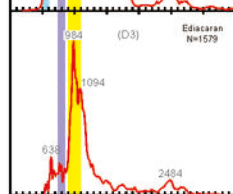
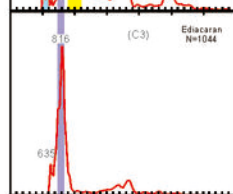
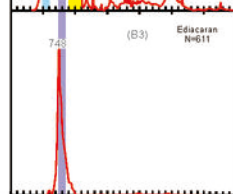
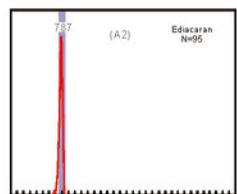
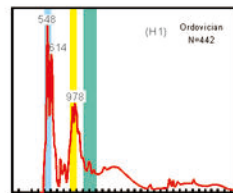
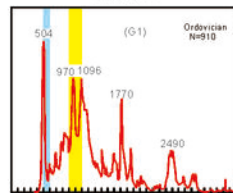
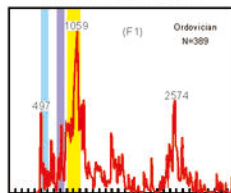
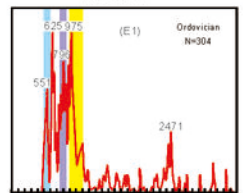
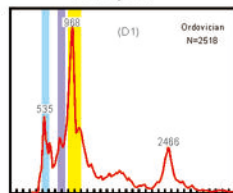
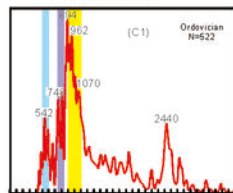
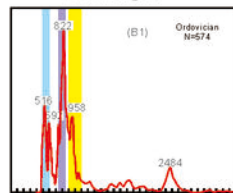
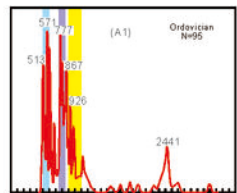


Figure 6.

820-600 Ma

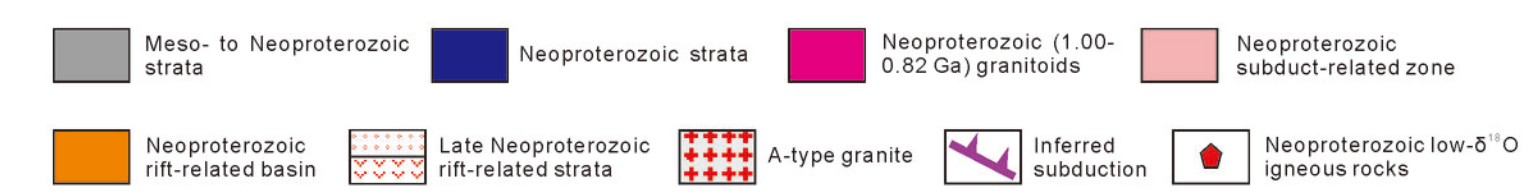
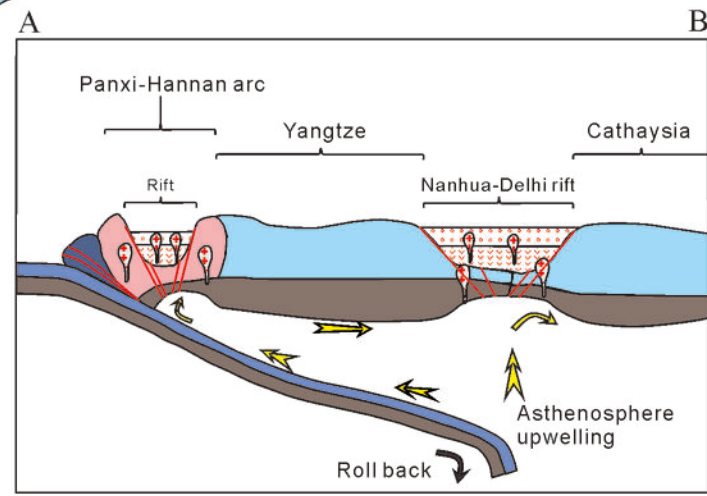
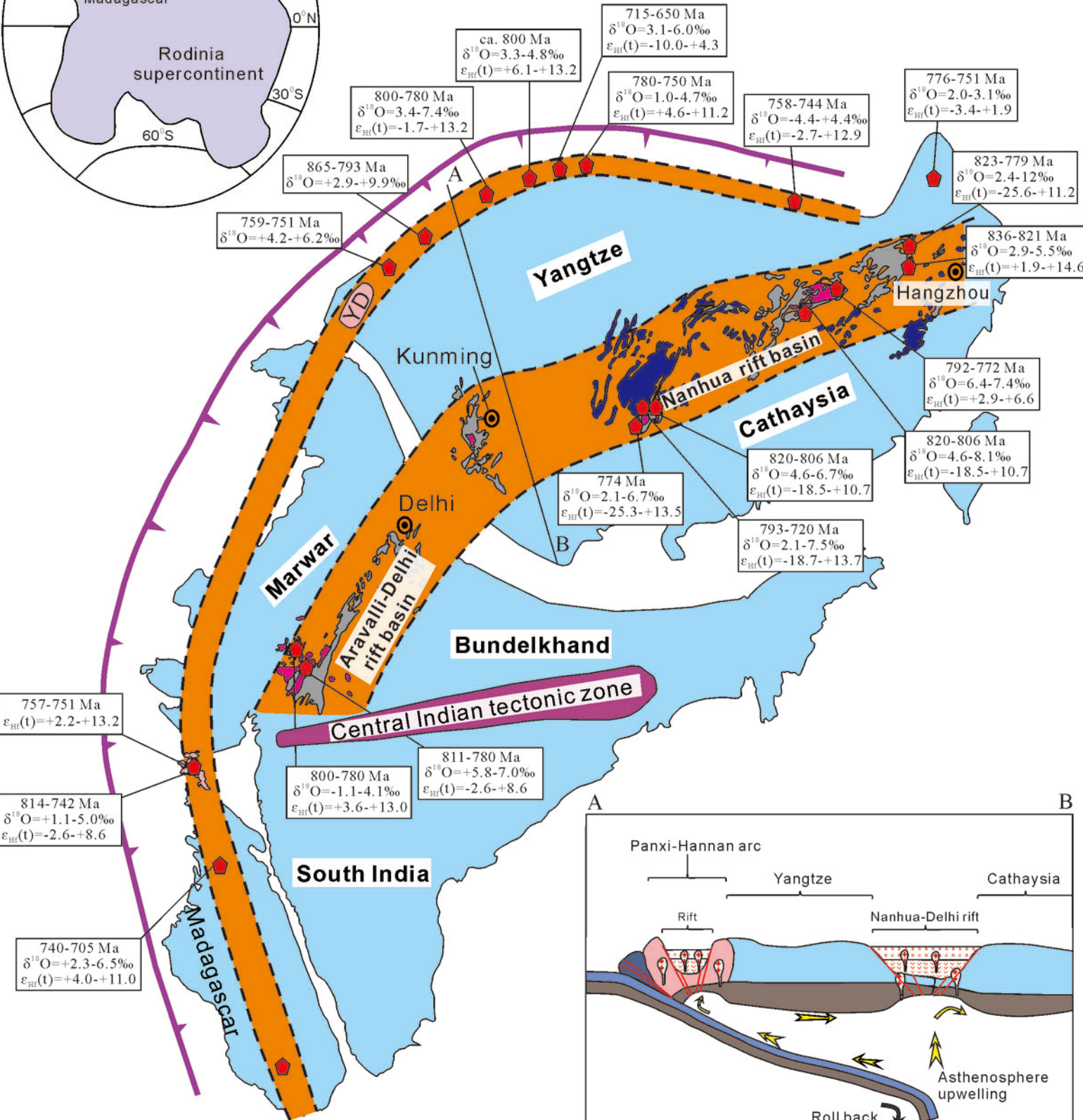
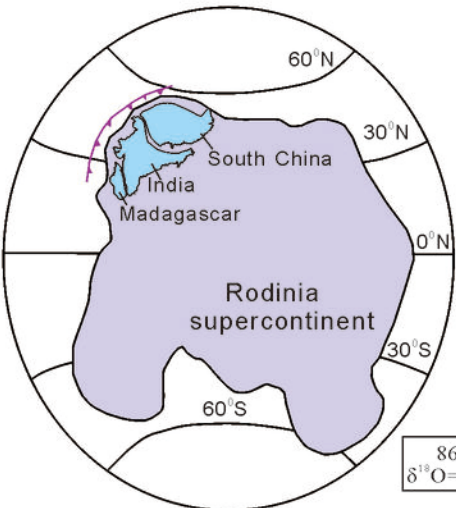


Figure 7.

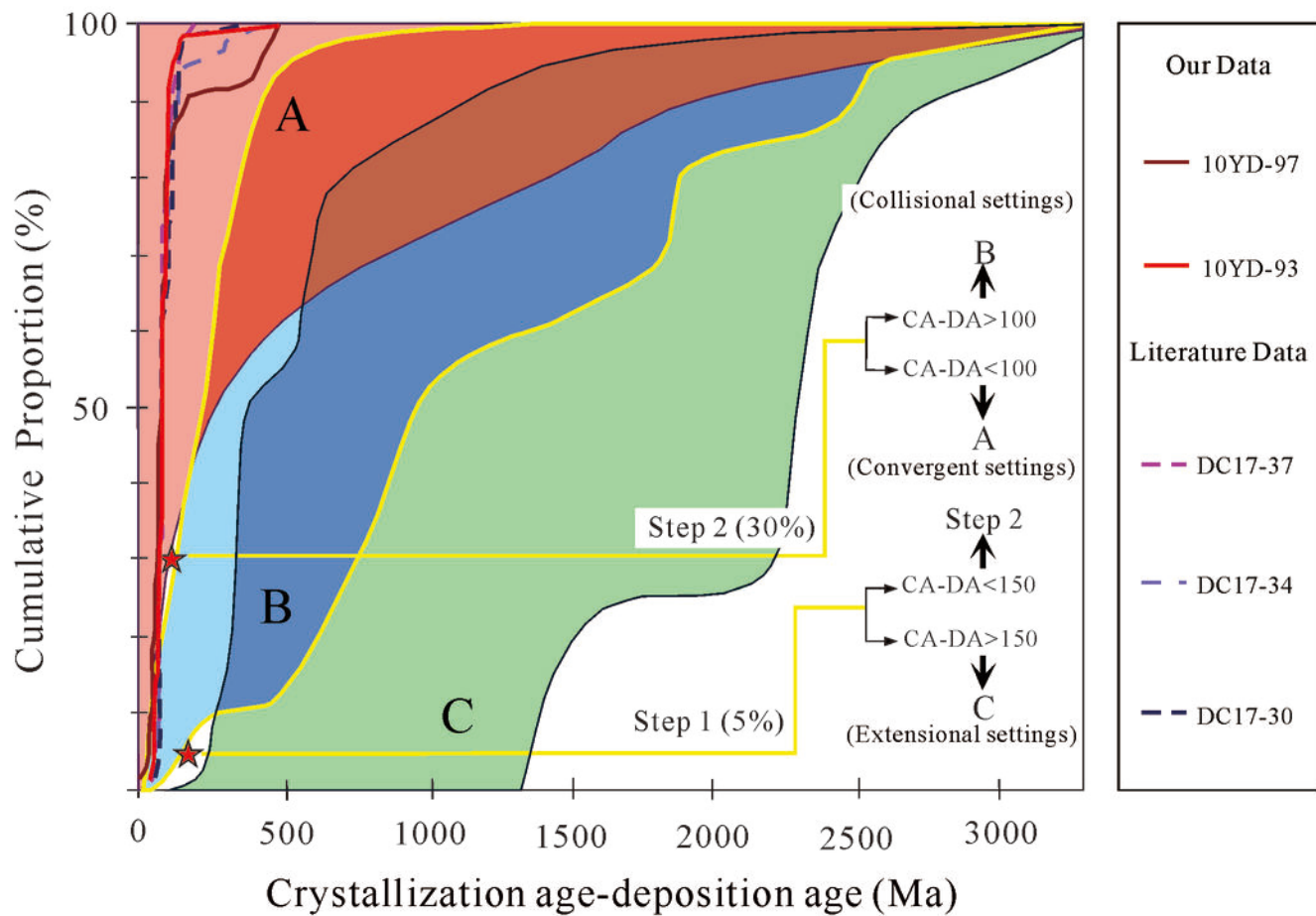
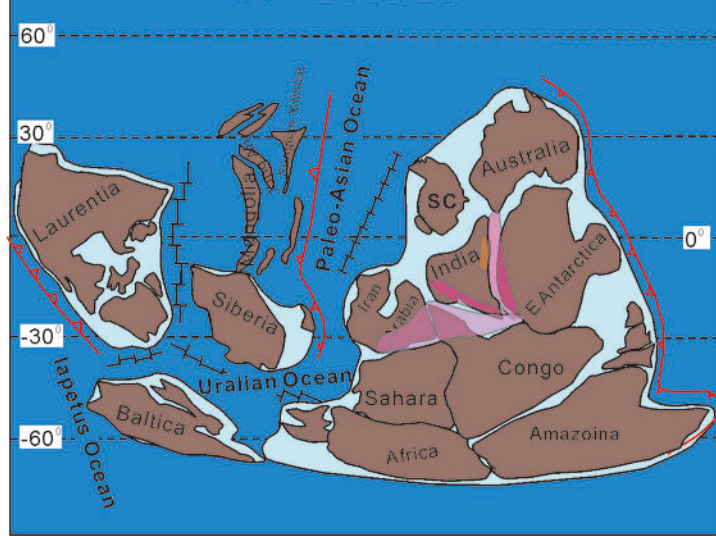
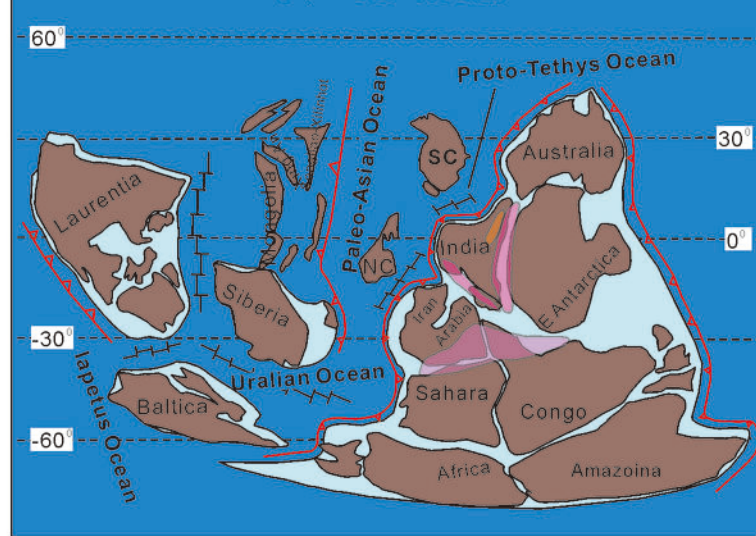


Figure 8.

(A) ~550-510 Ma



(B) ~510-460 Ma



East African Orogen Kuunga/Malagasy Orogen East Ghat Belt Ocean Spreading ridge Subducted zone

Table 1. Location and stratigraphic information of samples analyzed

Samples	Lithology	Latitude (N), Longitude (E)	Stratigraphic age	Mineral composition	Petrographical descriptions
10YD-93	Schist	N28°21.655, E100°13.619	The fourth member of Qiasi Group (Ptq ⁴ ; Cryogenian)	Quartz (80-85%), mica (5-10%), lithic fragment (1-5%) and minor heavy minerals	Fine-grained, subangular to subrounded, moderately to well sorted, grain-supported, moderately texture maturity
10YD-97	Schist	N28°22.453, E100°14.064	The third member of Qiasi Group (Ptq ³ ; Cryogenian)	Quartz (40-50%), mica (35-40%) and minor heavy minerals	Fine-grained, subangular to subrounded, moderately sorted, grain-supported, moderately texture maturity
10YD-99	Schist	N28°23.193, E100°14.410	Wachang Fm. (O ₁)	Quartz (60-65%), mica (20-35%), and minor heavy minerals	Fine-grained, subangular to subrounded, moderately to well sorted, grain-supported, moderately texture maturity
10YD-100	Sandstone	N28°24.153, E100°14.546	Dengying Fm. (Ediacaran)	Quartz (70-80%), feldspar (10-15%) and minor heavy minerals	Middle- and fine-grained, angular to subangular, moderately to poorly sorted, grain-supported, moderately to low texture maturity
10YD-102	Slate	N28°24.958, E100°14.405	Wachang Fm. (O ₁)	Quartz (ca. 70%), mica (20-25%), and minor heavy minerals	Fine-grained, subangular to subrounded, moderately sorted, matrix-supported, moderately texture maturity